GABA, glucose and insulin orchestrate CD4$^+$ T cells effector functions

Jin[1]# Z, Hammoud[1]# H, Bhandage[1] AK, Korol[1] SV, Trujeque-Ramos[1] O, Koreli[1] S., Chowdhury[1] AI, Sandbaumhüter[2] FA, Jansson[2] ET, Andrén[2] PE, Bergsten[1] P, Kamali-Moghaddam[3] M, Birnir* B

[1] Department of Medical Cell Biology, Uppsala University, Uppsala, Sweden

[2] Department of Pharmaceutical Biosciences, Uppsala University, Uppsala, Sweden.

[3] Department of Immunology, Genetics and Pathology, Science for Life Laboratory, Uppsala University, Uppsala, Sweden

 # Contributed equally

*** Correspondence**

Prof Bryndis Birnir

Department of Medical Cell Biology

Uppsala University

Uppsala, 75124, Sweden

Email: bryndis.birnir@mcb.uu.se

Tel: +46765620243

Abstract

Metabolic programs of immune cells are closely linked to their effector functions. Physiological molecules including glucose, insulin and γ-aminobutyric acid (GABA) provide environmental cues and guidance, although how they coordinate to regulate the cells is still being unraveled. Here, we demonstrate that GABA-mediated reduction of metabolic activity and release of inflammatory molecules, including IFNγ and IL-10, was abolished in human $CD4^+$ T cells when the glucose concentration was elevated above normal levels. Insulin enhanced the $GABA_A$ receptors-mediated currents and Ca^{2+} influx. GABA decreased, whereas insulin sustained glycolysis but in a SGLT (Na^+-glucose transporter)-dependent manner. In high glucose (16.7 mM), the SGLTs antagonist phlorizin alone or together with GABA restored the inhibition of IFNγ and IL-10 release. This study exposes concerted effects of GABA, glucose and insulin on $CD4^+$ T cells metabolic activity and release of inflammatory molecules, and identifies a role for SGLTs in $CD4^+$ T cells function.

40 **Introduction**

41 Human T cells are a crucial component of the adaptive immune response and provide essential
42 immune protection throughout life. Upon antigen stimulation, naïve T cells undergo clonal
43 expansion and further differentiate into effector cells. During this process, metabolic
44 reprogramming of T cells occurs and is intricately linked to their effector functions[1]. A variety
45 of soluble molecules including amino acids, other nutrients and hormones that are present in
46 blood, lymph nodes and tissue microenvironment influence T cell function[2-4]. γ-aminobutyric
47 acid (GABA), is primarily known as an inhibitory neurotransmitter in the central nervous
48 system, but is increasingly recognized as an immunomodulatory molecule[5-7]. We and others
49 have previously shown that GABA inhibits proliferation and cytokine secretion by activating
50 $GABA_A$ receptors in $CD4^+$ T cells[8-10]. The GABA concentration in the plasma from healthy
51 subjects is around 500 nM and increases somewhat in patients with Type 1 diabetes (T1D) or
52 major depression[10,11]. Glucose is the primary source of energy for activated T cells but is also
53 utilized for synthesizing biomolecules to support rapid proliferation and differentiation of the
54 cells[12,13]. At the time of activation, glucose is transported by facilitated glucose transporters
55 that equilibrate glucose across the cell membrane[3]. The blood glucose concentration varies
56 under physiological (around 5.6 mM) and pathophysiological conditions, for example, in
57 diabetes-related hypoglycemia (< 3 mM) or hyperglycemia (> 11 mM)[14]. In human clinical
58 trials, GABA treatment has been shown to be beneficial for glycemic control in T1D
59 individuals[15,16]. Insulin, a hormone mainly associated with glucose homeostasis[14], also
60 influences T cell function by modulating their metabolism[17] We and others have previously
61 demonstrated that GABA signaling regulates hormone secretion in human islets[18,19]. However,
62 how GABA, glucose and insulin orchestrate effective immune activities of T cells is still being
63 uncovered.

64 In the present study, we observe that, in human $CD4^+$ T cells, increasing the glucose
65 concentration above normal levels attenuates GABA-mediated inhibition of metabolic activity
66 and release of inflammatory proteins. Furthermore, insulin augments $GABA_A$ receptors-
67 mediated currents and Ca^{2+} influx in a manner that is dependent on the glucose concentration.
68 We also reveal the presence of functional Na^+-glucose transporter 2 (SGLT2) in activated $CD4^+$
69 T cells and, thereby, identify the possibility that T cells can raise the intracellular above the
70 environmental glucose concentration. Finally, we show that GABA, insulin, glucose and an
71 SGLT2 inhibitor differentially modulate glycolysis and release of IFNγ and IL-10 in activated
72 $CD4^+$ T cells. These results demonstrate coordinated influence of GABA, glucose and insulin on
73 metabolic activity and release of inflammatory proteins, and highlight the involvement of
74 SGLTs in $CD4^+$ T cell functions.
75
76 **Results**
77 **GABA inhibition of activated T cell function is affected by glucose**
78 Physiological blood glucose concentration 2h after a meal, is normally maintained
79 around 5.6 mM in healthy individuals, while it is higher in diseases such as diabetes (> 7 mM)[14]
80 or Covid-19[20]. Metabolic activity of T cells is closely related to their function[1]. The
81 physiological GABA concentration in human plasma is about 500 nM[10,21] and it provides a
82 homeostatic inhibition on T cells[10]. The culture media (e.g., RPMI1640) commonly used for *in*
83 *vitro* T cell assays usually contain high glucose concentration (> 10 mM). Therefore, we
84 examined effects of four glucose concentrations on the GABA inhibition of metabolic activity
85 of $CD4^+$ T cells (N=35–53 human donors; Fig. 1a; Supplementary Table 1, Supplementary Fig.
86 1). At glucose concentrations higher than the physiological level (10 mM and 16.7 mM), the
87 inhibition by GABA (500 nM) was abolished (Fig. 1a). In absence of GABA, the metabolic

88 activity of activated $CD4^+$ T cells varied somewhat for the different glucose concentrations (5
89 mM vs. 2.8 or 10 mM; Supplementary Fig. 2a). When the GABA responses were compiled
90 based on low-normal (2.8 mM, 5.6 mM) or high (10 mM, 16.7 mM) glucose concentrations, a
91 clear shift was observed for GABA's inhibitory response (Fig. 1b). At the level 0.9 or lower
92 metabolic activity (Fig. 1b), cells from 74% of the donors were inhibited by GABA in the low-
93 normal glucose group. The metabolic activity of cells from these same donors were not
94 inhibited at the higher glucose concentrations (Fig. 1c). In contrast, cells from the remaining
95 26% donors were not inhibited by GABA at any glucose concentration (Supplementary Fig.
96 2b), in agreement with previous report [10]. Intrigued by these results, we sought whether
97 glucose affected other immunological functions regulated by GABA. Since glycolysis feeds
98 substrates into anabolic metabolism, we studied if glucose modulated the GABA-inhibition of
99 release of biomolecules from $CD4^+$ T cells from the same donors (N=17) cultured in low-normal
100 or high glucose. In each sample, 92 inflammation-related biomolecules commonly associated
101 with inflammation were measured using Olink Target Inflammation protein panel, which is
102 based on the multiplex proximity extension assay (PEA) technology. A total of 59 different
103 proteins were detected. Similar to the results from the metabolic activity, the GABA-inhibition
104 of proteins released from $CD4^+$ T cells was glucose concentration-dependent (Fig. 1d). The
105 GABA inhibition was optimal at the physiological glucose concentration (5.6 mM), where
106 GABA decreased the release of 37 proteins. In contrast, GABA did not affect release of
107 proteins in neither 10 mM nor 16.7 mM glucose (Fig. 1d). ELISA confirmed the PEA results for
108 two cytokines; interferon gamma (IFNγ), the principal cytokine of $CD4^+$ T helper1 cells and
109 interleukin-10 (IL-10), the principal cytokine for $CD4^+$ T helper2 and T regulatory cells (Fig. 1e,
110 f). Further, in absence of GABA, increasing the glucose concentration alone enhanced release

111 of IFNγ (Supplementary Fig. 2c) but not IL-10 (Supplementary Fig. 2d). Thus, GABA-dependent
112 regulation of $CD4^+$ T cells is linked to the extracellular glucose concentration.

113 **Insulin enhances the GABA-activated currents and modulates $GABA_A$ receptor expression in**
114 **$CD4^+$ T cells**

115 Glucose homeostasis is influenced by a variety of hormones, with insulin being one of
116 the key players. Interestingly, at least in excitable cells, insulin is also a regulator of GABA
117 signaling[22-24]. The insulin receptor is not expressed in resting T cells but is prominent at 48 h
118 post-activation[17]. Therefore, after 48-h activation, we incubated $CD4^+$ T cells with insulin at
119 physiologically relevant concentration (3 nM) and where unspecific activation of other
120 receptors-types does not take place[17,24]. GABA activates two types of receptors in cell
121 membranes; the $GABA_A$ receptor ($GABA_AR$), a pentameric chloride ion channel, that opens
122 when GABA binds to the receptor and the $GABA_B$ receptor ($GABA_BR$), a G-protein coupled
123 receptor, that is formed as a dimer**.** To-date, only one of the two $GABA_B$ isoforms required for
124 function has been detected in immune cells, whereas several $GABA_A$ receptor subunits are
125 identified in T cells[4,10]. We measured the GABA-activated $GABA_AR$ currents in intact activated
126 $CD4^+$ cells using perforated patch-clamp electrophysiology (Fig. 2a, b, c, d). Since the
127 intracellular environment is unchanged, intracellular signaling that may take place is expected
128 to function normally. The 500 nM GABA-activated $GABA_AR$-mediated currents were blocked
129 by the $GABA_AR$ antagonist picrotoxin. Picrotoxin is a specific, open channel blocker of $GABA_A$
130 receptors[25]. These maximal current responses were only enhanced by insulin at 5.6 mM but
131 not at 16.7 mM glucose (Fig 2a), but the apparent GABA affinity (EC_{50}) for $GABA_AR$ was similar
132 in 5.6 mM and 16.7 mM glucose, 0.7 nM and 0.9 nM GABA, respectively (Fig. 2b). Insulin then
133 shifted the EC_{50} values more than 10-fold, to 0.04 nM and 0.06 nM GABA (Fig. 2c), for the two
134 glucose concentrations, respectively. These results suggest that insulin increases the $GABA_AR$

135 plasma membrane surface number in 5.6 mM glucose but enhances the GABA affinity of
136 $GABA_AR$ in $CD4^+$ T cells at both glucose concentrations. The $GABA_AR$ agonists muscimol and
137 TACA evoked currents similar to GABA (Fig. 2d). The currents reversed at −37 mV
138 (Supplementary Fig. 3a), close to the calculated reversal potential for chloride (E_{Cl} = −39 mV).
139 By regulating the membrane potential these very sensitive $GABA_AR$ channels may affect
140 activity of other ion channels or flow of ions across the cell membrane[26].

141 Among the 19 $GABA_AR$ subunits, the $GABA_AR$ ρ2 (*GABRR2*) is a highly expressed subunit
142 in peripheral blood mononuclear cells[10]. We therefore examined the ρ2 mRNA and protein
143 expression levels in $CD4^+$ T cells. Irrespective of glucose concentration, activation of $CD4^+$ T
144 cells decreased the expression of the *GABRR2* transcript relative to resting cells, whereas
145 insulin increased the expression of the *GABRR2* (Fig. 2e). In $CD4^+$ T cells fluorescent labelling
146 of the GABRR2 was detected by specific antibody (Fig. 2f, g). Taken together, the data show
147 that insulin potentiates GABA signaling in activated $CD4^+$ T cells by enhancing ρ2-containing
148 $GABA_AR$ expressed in the cells.

149 **Insulin enhances GABA-activated Ca^{2+} entry in $CD4^+$ T cell**

150 The cytoplasmic concentration of Ca^{2+} ions is tightly regulated in T cells but can be
151 increased by release from intracellular stores or by entry through plasma membrane Ca^{2+} ion
152 channels[27]. A representative live cell-Ca^{2+} recording trace measured from activated $CD4^+$ T
153 cells (Fig. 3a) showed that acute GABA (500 nM) application induced transient calcium signal,
154 which was, in fact, influx of extracellular calcium and not due to release from intracellular
155 stores as no signal could be detected in absence of extracellular calcium (Fig. 3a). Analyzed
156 live cell-Ca^{2+} recording data from four donors is shown in Fig. 3b. Transient change in glucose
157 from 5.6 to 16.7 mM did not alter the 500 nM GABA-activated Ca^{2+} response (Supplementary
158 Fig. 3b). Insulin incubation of cells enhanced the physiological saturating (500 nM) GABA-

159 induced Ca^{2+} signals in 5.5 mM but not in 16.7 mM glucose (Fig. 3c), whereas no differences
160 were observed for baseline Ca^{2+} levels in cells with or without insulin incubation
161 (Supplementary Fig. 3c). The GABA-activated Ca^{2+} signal was blocked by the $GABA_AR$
162 antagonist picrotoxin (Fig. 3d), while no effect was observed by the $GABA_BR$ antagonist,
163 CGP52432 (Supplementary Fig. 3d). This prompted us to examine dose-response relationship
164 between GABA and the Ca^{2+} signals in cells with or without insulin incubation (Fig. 3e, f, g;
165 Supplementary Fig. 3e). Representative time-lapse recording of a $CD4^+$ T cell, 16.7 mM
166 glucose, with insulin, demonstrates that raising GABA concentrations induced increasing Ca^{2+}
167 signals (Fig. 3e). Insulin incubation of the cells lowered the EC_{50} values of the GABA-activated
168 Ca^{2+} signals. The apparent GABA affinity of the Ca^{2+} signal was 40 nM and 133 nM GABA in 5.5
169 mM and 16.7 mM glucose, and shifted more than 1000-fold to 0.01 nM and 0.086 nM GABA
170 with insulin, respectively (Fig. 3f, g). The GABA-induced Ca^{2+} response and enhancement by
171 insulin is in accordance with our electrophysiological patch-clamp data (Fig. 2a, b, c). These
172 data demonstrate that physiological GABA (pM – nM) increases Ca^{2+} entry, and the response
173 is profoundly enhanced after insulin treatment.

174 **$GABA_AR$ mediates GABA-activated Ca^{2+} entry in $CD4^+$ T cells**

175 To confirm the $GABA_AR$ connection in the evoked Ca^{2+} signal, we further examined the
176 Ca^{2+} response to $GABA_AR$ agonists and antagonists. The application of $GABA_AR$ agonists,
177 muscimol (Fig. 4a) or TACA (Fig. 4b) increased relative Ca^{2+} signals, which were inhibited by
178 $GABA_AR$ antagonists, TPMPA (Fig. 4c) or picrotoxin (Fig. 4a, b, c), in activated $CD4^+$ T cells
179 treated with or without insulin. TACA and TPMPA are more selective for ρ-containing
180 $GABA_AR$[25,28,29]. Ca^{2+} release-activated Ca^{2+} (CRAC) channels mediate store operated calcium
181 entry (SOCE) in T cells that is central to the Ca^{2+} homeostasis and cytoplasmic Ca^{2+} levels[27].
182 The GABA-activated Ca^{2+} signal was inhibited by 1 μM YM48583 (Fig. 4d), an antagonist of

183 SOCE, revealing the Ca^{2+} ion channel participating in the cascade. The tight scaling of the Ca^{2+}
184 signal from $GABA_AR$ activation to Ca^{2+} entry and the sensitization by insulin identifies a specific,
185 focused mechanism regulating Ca^{2+} signaling in $CD4^+$ T cells.

186 Insulin is known to regulate intracellular signaling and gene expression, whereas less
187 is known about effects of GABA. However, out of the nine examined genes encoding
188 transcription factors or kinases, only *NFATC2* (nuclear factor of activated T cells 2) was
189 significantly reduced by GABA at 5.6 mM glucose (Supplementary Table 2). NFATs proteins are
190 activated by increased Ca^{2+} in the cytoplasm and translocate to the nucleus, where they
191 regulate transcription of many proteins including inflammatory molecules[30].

192 **GABA regulation of glycolysis is glucose-dependent**

193 That GABA regulated expression of signaling pathways and proteins was revealed by
194 mass spectrometry (MS) of activated $CD4^+$ T cells cultured in the presence or absence of GABA
195 (Fig. 5a, Supplementary Table 3). Hexokinase 1 (HK1), the first enzyme in the glycolytic
196 pathway, was significantly down-regulated by GABA in both 5.6 mM and 16.7 mM glucose
197 (Fig. 5b). HK activity was negligible under resting conditions but increased about 60 times in
198 activated $CD4^+$ T cells in both 5.6 mM and 16.7 mM glucose. Intriguingly, GABA decreased the
199 HK activity only at 5.6 mM glucose and insulin had no further effect (Fig. 5c). T cells switch to
200 aerobic glycolysis upon activation as their predominant way to generate adenosine 5´-
201 triphosphate (ATP) and to accumulate biomass[31,32], the so-called Warburg effect. It results in
202 glucose-derived pyruvate being converted to lactate that can be detected by measuring
203 extracellular acidification rate (ECAR)[33]. Since HK is the gate-keeper for the glycolytic pathway,
204 we examined if glucose, GABA or insulin modulated glycolysis. Representative ECAR traces
205 and average values for activated $CD4^+$ T cells at 5.6 mM and 16.7 mM glucose in the presence
206 or absence of GABA and insulin are shown in Fig. 5d and e. GABA but not insulin inhibited

207 glycolysis and glycolytic capacity but only in 5.6 mM glucose. No effect of GABA at higher
208 glucose suggested the possibility that either the intracellular glucose might affect the GABA
209 inhibition of glycolysis or there were other competing mechanisms at work.

210 **Functional SGLT2 modulates glycolysis and cytokine release in activated CD4$^+$ T cells**

211 Facilitated glucose transport is the main route for glucose entry into activated T cells[3].
212 We confirmed the dominance of the facilitated transport on the cellular metabolic activity of
213 activated CD4$^+$ T cells (Fig. 6a) by examining the effects of antagonists of glucose transporters,
214 WZB117, an inhibitor of the facilitated glucose transporters (GLUTs), , and phlorizin, an
215 inhibitor of Na^+-dependent glucose transport (SGLT1 and SGLT2)[34]. WZB117 decreased
216 whereas phlorizin had no effect at either glucose concentration on the metabolic activity of
217 the T cells (Fig. 6a). In accordance, our RNAseq analysis showed several facilitated GLUTs gene
218 transcripts (e.g., *SLC2A1* and *SLC2A3*) were prominently expressed in activated CD4$^+$ T cells
219 (Fig. 6b). Nevertheless, *SLC5A2*, the gene encoding the sodium-dependent glucose transporter
220 SGLT2, was also detected at a modest level (Fig. 6b). Western blot and immunofluorescence
221 staining data showed protein expression of SGLT2 in the cells (Fig. 6c, d).

222 In presence of phlorizin or empagliflozin, another SGLT2 antagonist and a prescription
223 medicine in type 2 diabetes, a significant reduction in glucose uptake was observed in insulin
224 incubated cells (Fig. 7a). Phlorizin alone reduced glycolysis and glycolytic capacity at both 5.6
225 mM and 16.7 mM glucose (Fig. 7b), whereas insulin reduced or abolished the inhibition by
226 phlorizin (Fig. 7b). Since phlorizin reduced glycolysis, it could be expected to reduce synthesis
227 of biomolecules such as IFNγ and IL-10, similar effects to what we observed for GABA (see
228 Figs. 1d, e, f). Indeed, phlorizin reduced release of IFNγ and IL-10 at both 5.6 mM and 16.7 mM
229 glucose even in the presence of insulin (Fig. 8a, b) with the exception of IFNγ at 16.7 mM
230 glucose with insulin, where only phlorizin together with GABA reduced IFNγ release,

231 approximately 50%. In general, there was a trend for GABA to enhance the phlorizin reduction
232 of release of IFNγ and IL-10. The results demonstrate functional Na^+-dependent glucose
233 carriers in $CD4^+$ T cells and identify their relevance for production of cytokines.

234 **Discussion**

235 T cells modulate their metabolism to adapt to different environments[1,31,32]. When
236 $CD4^+$ T cells are activated, their metabolic activity is altered to meet the demands of cell
237 growth, proliferation and effector functions. Here we revealed that GABA, glucose and insulin
238 together orchestrate functions of $CD4^+$ T cell, to-coordinate and to-set the activity level of
239 distinct cellular pathways linked to glucose metabolism and that are central for T cells effector
240 functions (Fig. 9).

241 Proliferating T cells shift their metabolic phenotype to aerobic glycolysis at the expense
242 of mitochondrial oxidative phosphorylation[31,35]. Although this switch is inefficient in terms of
243 generating ATP, it confers advantage for the biosynthetic pathways that branch out from
244 glycolysis[31,32]. GABA decreased cellular metabolic activity and release of proteins in a glucose
245 concentration-dependent manner. Insulin shifted the $GABA_AR$ signaling by making it
246 supersensitive to GABA and consequently enhanced Ca^{2+} entry through CRAC channels, an
247 elegant way of modulating intracellular Ca^{2+} levels and intracellular processes affecting T cells
248 effector functions.

249 CRAC channel-mediated SOCE regulates several Ca^{2+} signaling downstream pathways
250 including the expression of facilitated glucose transporters (e.g., GLUT1) and glycolytic
251 enzymes such as HK via activation of transcriptional factor NFAT in T cells[30]. Our data show
252 that GABA decreases the expression of *NFATC2* mRNA transcript and the activity of HK2 at 5.6
253 mM glucose in activated $CD4^+$ T cells. Consequently, at the level of HK there is a cross-over of
254 GABA signaling and glucose transport for regulating glycolysis and, thereby, effector functions

255 of T cells. Although glucose transport in $CD4^+$ T cells is mainly mediated by facilitated glucose
256 transporters, the present results identified significant Na^+-dependent glucose (SGLT2)
257 transport. This is highly relevant for the effector functions as only SGLTs can raise the
258 intracellular glucose level above the extracellular ones. HK is the first enzyme in the glycolytic
259 pathway and by converting glucose to glucose-6-phosphate (G-6-P), traps glucose within the
260 cell[7]. Human HK has normally maximum activity in 5 mM glucose in the presence of natural
261 inhibitors, such as G-6-P[36], but HK activity is increased at glucose concentrations > 5 mM[36].
262 This is in line with our results, where GABA only succeeded decreasing HK enzymatic activity
263 in 5.6 mM glucose. Na^+-dependent glucose transport drives glucose into cells even at high
264 intracellular glucose concentrations[34]. Glucose competes with G-6-P for the binding site on
265 HK[36], decreasing the inhibition of HK[36], which results in increased substrate availability for
266 biosynthesis as the intracellular glucose concentration increases[13]. Aerobic glycolysis directly
267 regulates synthesis of IFNγ[37] by engaging glyceraldehyde-3-phosphate dehydrogenase
268 (GDPDH) and, thereby, relieving its inhibition of IFNγ mRNA translation. In concordance,
269 activated $CD4^+$ cells secreted more IFNγ in high glucose. GABA promoted a glycolytic switch to
270 lower values for both glycolysis and the glycolytic capacity in 5.6 mM glucose that was gone
271 in 16.7 mM glucose, whereas phlorizin was effective inhibitor at both glucose concentrations
272 and, in particular, in the absence of insulin. Discovering that $GABA_AR$ activation together with
273 SGLT2 inhibition can dramatically reduce the levels of IFNγ and IL-10, at both normal and high
274 glucose concentrations, has implications for regulation of inflammation, as availability of
275 biosynthetic intermediates-production fuels effector signaling molecules and functions[13].

276 $GABA_ARs$ are widespread in the brain and are present in many other tissues[38] but
277 $GABA_ARs$ containing GABRR2 (ρ2 subunit) are rare outside the immune system, with the
278 exception of the retina[39]. $GABA_AR$-ρ2 might be a valuable and a rather specific drug target[28].

279 SGLT2 inhibitors such as empagliflozin, are already in clinical use[40] and might be considered
280 to cover new areas of application. Strengthening the GABA response and inhibiting SGLT2 in
281 $CD4^+$ T cells might be valuable tools[15,41,42], when regulating inflammation is desirable.

282 In conclusion, physiological factors such as glucose, GABA and insulin guide the
283 adaptation of $CD4^+$ T cells and modify their effector functions. The reduction of metabolic
284 activity and release of inflammatory molecules in response to GABA or SGLT2 inhibitors,
285 revealed a switch that can be turned on or off. The study unveils the mechanisms of GABA
286 modulation of $CD4^+$ T cells and identifies a critical role for SGLTs in immune function. The
287 results have implications for treatment of a number of diseases including diabetes but also
288 maladies such as Covid-19 and cytokine storm, inflammatory diseases and cancer.

289

290 **Acknowledgements:** We thank the following for support; The Swedish Children's Diabetes
291 Foundation, The Swedish Diabetes Foundation, The Swedish Research Council 2018-02952,
292 EXODIAB, The Ernfors Foundation and The Thurings Foundation. We thank Dr Zhitao Gong
293 for participation in some of the experiments and Universitetslektor Femke Heindryckx for the
294 gift of the HepG2 cell line.

295 **Author Contributions:** BB, ZJ, HH conceived project; HH, ZJ, AKB, SVK, BB, MKM
296 designed experiments; HH, ZJ, AKB, SVK, OTR, SK, AIC and FA did experiments; ZJ, HH,
297 AKB, SVK made figures; all authors analyzed results, BB wrote manuscript that was edited by
298 ZJ, HH, AKB and then commented on by all authors.

299 **Competing interests**: BB has patent applications WO2019/164446A1 and WO2019162403A1

300

301 **References**

302 1 Geltink, R. I. K., Kyle, R. L. & Pearce, E. L. Unraveling the Complex Interplay Between T
303 Cell Metabolism and Function. *Annu Rev Immunol* **36**, 461-488 (2018).
304 https://doi.org:10.1146/annurev-immunol-042617-053019
305 2 van Niekerk, G., Christowitz, C., Conradie, D. & Engelbrecht, A. M. Insulin as an
306 immunomodulatory hormone. *Cytokine Growth Factor Rev* **52**, 34-44 (2020).
307 https://doi.org:10.1016/j.cytogfr.2019.11.006
308 3 Song, W., Li, D., Tao, L., Luo, Q. & Chen, L. Solute carrier transporters: the metabolic
309 gatekeepers of immune cells. *Acta Pharm Sin B* **10**, 61-78 (2020).
310 https://doi.org:10.1016/j.apsb.2019.12.006
311 4 Barragan, A., Weidner, J. M., Jin, Z., Korpi, E. R. & Birnir, B. GABAergic signalling in the
312 immune system. *Acta Physiol (Oxf)* **213**, 819-827 (2015).
313 https://doi.org:10.1111/apha.12467
314 5 Tian, J. & Kaufman, D. L. The GABA and GABA-Receptor System in Inflammation, Anti-
315 Tumor Immune Responses, and COVID-19. *Biomedicines* **11** (2023).
316 https://doi.org:10.3390/biomedicines11020254
317 6 Fu, J. *et al.* GABA regulates IL-1beta production in macrophages. *Cell Rep* **41**, 111770
318 (2022). https://doi.org:10.1016/j.celrep.2022.111770
319 7 Zhang, B. *et al.* B cell-derived GABA elicits IL-10(+) macrophages to limit anti-tumour
320 immunity. *Nature* **599**, 471-476 (2021). https://doi.org:10.1038/s41586-021-04082-1
321 8 Tian, J. *et al.* Gamma-aminobutyric acid inhibits T cell autoimmunity and the
322 development of inflammatory responses in a mouse type 1 diabetes model. *J Immunol*
323 **173**, 5298-5304 (2004). https://doi.org:173/8/5298 [pii]
324 9 Bjurstom, H. *et al.* GABA, a natural immunomodulator of T lymphocytes. *J*
325 *Neuroimmunol* **205**, 44-50 (2008). https://doi.org:S0165-5728(08)00389-5 [pii]
326 10.1016/j.jneuroim.2008.08.017
327 10 Bhandage, A. K. *et al.* GABA Regulates Release of Inflammatory Cytokines From
328 Peripheral Blood Mononuclear Cells and CD4(+) T Cells and Is Immunosuppressive in
329 Type 1 Diabetes. *EBioMedicine* **30**, 283-294 (2018).
330 https://doi.org:10.1016/j.ebiom.2018.03.019
331 11 Bhandage, A. K. *et al.* Depression, GABA, and Age Correlate with Plasma Levels of
332 Inflammatory Markers. *Int J Mol Sci* **20** (2019). https://doi.org:10.3390/ijms20246172
333 12 Macintyre, A. N. *et al.* The glucose transporter Glut1 is selectively essential for CD4 T
334 cell activation and effector function. *Cell Metab* **20**, 61-72 (2014).
335 https://doi.org:10.1016/j.cmet.2014.05.004
336 13 Lunt, S. Y. & Vander Heiden, M. G. Aerobic glycolysis: meeting the metabolic
337 requirements of cell proliferation. *Annu Rev Cell Dev Biol* **27**, 441-464 (2011).
338 https://doi.org:10.1146/annurev-cellbio-092910-154237
339 14 Niswender, K. D. Basal insulin: physiology, pharmacology, and clinical implications.
340 *Postgrad Med* **123**, 17-26 (2011). https://doi.org:10.3810/pgm.2011.07.2300
341 15 Espes, D. *et al.* GABA induces a hormonal counter-regulatory response in subjects with
342 long-standing type 1 diabetes. *BMJ Open Diabetes Res Care* **9** (2021).
343 https://doi.org:10.1136/bmjdrc-2021-002442
344 16 Rabinovitch, A. *et al.* Efficacy of combination therapy with GABA, a DPP-4i and a PPI as
345 an adjunct to insulin therapy in patients with type 1 diabetes. *Front Endocrinol*
346 *(Lausanne)* **14**, 1171886 (2023). https://doi.org:10.3389/fendo.2023.1171886

17 Tsai, S. *et al.* Insulin Receptor-Mediated Stimulation Boosts T Cell Immunity during Inflammation and Infection. *Cell Metab* **28**, 922-934 e924 (2018). https://doi.org:10.1016/j.cmet.2018.08.003

18 Braun, M. *et al.* Gamma-aminobutyric acid (GABA) is an autocrine excitatory transmitter in human pancreatic beta-cells. *Diabetes* **59**, 1694-1701 (2010). https://doi.org:db09-0797 [pii]
10.2337/db09-0797

19 Korol, S. V. *et al.* Functional Characterization of Native, High-Affinity GABAA Receptors in Human Pancreatic beta Cells. *EBioMedicine* **30**, 273-282 (2018). https://doi.org:10.1016/j.ebiom.2018.03.014

20 Codo, A. C. *et al.* Elevated Glucose Levels Favor SARS-CoV-2 Infection and Monocyte Response through a HIF-1alpha/Glycolysis-Dependent Axis. *Cell Metab* **32**, 498-499 (2020). https://doi.org:10.1016/j.cmet.2020.07.015

21 Li, J. *et al.* Study of GABA in Healthy Volunteers: Pharmacokinetics and Pharmacodynamics. *Front Pharmacol* **6**, 260 (2015). https://doi.org:10.3389/fphar.2015.00260

22 Wan, Q. *et al.* Recruitment of functional GABA(A) receptors to postsynaptic domains by insulin. *Nature* **388**, 686-690 (1997). https://doi.org:10.1038/41792

23 Xu, E. *et al.* Intra-islet insulin suppresses glucagon release via GABA-GABAA receptor system. *Cell Metab* **3**, 47-58 (2006). https://doi.org:10.1016/j.cmet.2005.11.015

24 Jin, Z. *et al.* Insulin reduces neuronal excitability by turning on GABA(A) channels that generate tonic current. *Plos One* **6**, e16188 (2011). https://doi.org:10.1371/journal.pone.0016188

25 Cowgill, J. *et al.* Structure and dynamics of differential ligand binding in the human rho-type GABA(A) receptor. *Neuron* (2023). https://doi.org:10.1016/j.neuron.2023.08.006

26 Cahalan, M. D. & Chandy, K. G. The functional network of ion channels in T lymphocytes. *Immunol Rev* **231**, 59-87 (2009). https://doi.org:10.1111/j.1600-065X.2009.00816.x

27 Vaeth, M., Kahlfuss, S. & Feske, S. CRAC Channels and Calcium Signaling in T Cell-Mediated Immunity. *Trends Immunol* **41**, 878-901 (2020). https://doi.org:10.1016/j.it.2020.06.012

28 Naffaa, M. M., Hibbs, D. E., Chebib, M. & Hanrahan, J. R. Pharmacological Effect of GABA Analogues on GABA-varrho2 Receptors and Their Subtype Selectivity. *Life (Basel)* **12** (2022). https://doi.org:10.3390/life12010127

29 Naffaa, M. M., Hung, S., Chebib, M., Johnston, G. A. R. & Hanrahan, J. R. GABA-rho receptors: distinctive functions and molecular pharmacology. *Br J Pharmacol* **174**, 1881-1894 (2017). https://doi.org:10.1111/bph.13768

30 Vaeth, M. *et al.* Store-Operated Ca(2+) Entry Controls Clonal Expansion of T Cells through Metabolic Reprogramming. *Immunity* **47**, 664-679 e666 (2017). https://doi.org:10.1016/j.immuni.2017.09.003

31 Pearce, E. L., Poffenberger, M. C., Chang, C. H. & Jones, R. G. Fueling immunity: insights into metabolism and lymphocyte function. *Science* **342**, 1242454 (2013). https://doi.org:10.1126/science.1242454

32 Jones, W. & Bianchi, K. Aerobic glycolysis: beyond proliferation. *Front Immunol* **6**, 227 (2015). https://doi.org:10.3389/fimmu.2015.00227

392 33 Traba, J., Miozzo, P., Akkaya, B., Pierce, S. K. & Akkaya, M. An Optimized Protocol to
393 Analyze Glycolysis and Mitochondrial Respiration in Lymphocytes. *J Vis Exp* (2016).
394 https://doi.org:10.3791/54918
395 34 Hummel, C. S. *et al.* Glucose transport by human renal Na+/D-glucose cotransporters
396 SGLT1 and SGLT2. *Am J Physiol Cell Physiol* **300**, C14-21 (2011).
397 https://doi.org:10.1152/ajpcell.00388.2010
398 35 Michalek, R. D. *et al.* Cutting edge: distinct glycolytic and lipid oxidative metabolic
399 programs are essential for effector and regulatory CD4+ T cell subsets. *J Immunol* **186**,
400 3299-3303 (2011). https://doi.org:10.4049/jimmunol.1003613
401 36 Fujii, S. & Beutler, E. High glucose concentrations partially release hexokinase from
402 inhibition by glucose 6-phosphate. *Proc Natl Acad Sci U S A* **82**, 1552-1554 (1985).
403 https://doi.org:10.1073/pnas.82.5.1552
404 37 Chang, C. H. *et al.* Posttranscriptional control of T cell effector function by aerobic
405 glycolysis. *Cell* **153**, 1239-1251 (2013). https://doi.org:10.1016/j.cell.2013.05.016
406 38 Young, S. Z. & Bordey, A. GABA's control of stem and cancer cell proliferation in adult
407 neural and peripheral niches. *Physiology (Bethesda)* **24**, 171-185 (2009).
408 https://doi.org:10.1152/physiol.00002.2009
409 39 Bailey, M. E., Albrecht, B. E., Johnson, K. J. & Darlison, M. G. Genetic linkage and
410 radiation hybrid mapping of the three human GABA(C) receptor rho subunit genes:
411 GABRR1, GABRR2 and GABRR3. *Biochim Biophys Acta* **1447**, 307-312 (1999).
412 https://doi.org:10.1016/s0167-4781(99)00167-0
413 40 Packer, M. *et al.* Cardiovascular and Renal Outcomes with Empagliflozin in Heart
414 Failure. *N Engl J Med* **383**, 1413-1424 (2020).
415 https://doi.org:10.1056/NEJMoa2022190
416 41 Masoodi, M. *et al.* Disturbed lipid and amino acid metabolisms in COVID-19 patients. *J*
417 *Mol Med (Berl)* (2022). https://doi.org:10.1007/s00109-022-02177-4
418 42 Alshnbari, A. & Idris, I. Can sodium-glucose co-transporter-2 (SGLT-2) inhibitor reduce
419 the risk of adverse complications due to COVID-19? - Targeting hyperinflammation.
420 *Curr Med Res Opin* **38**, 357-364 (2022).
421 https://doi.org:10.1080/03007995.2022.2027141
422
423
424

Figure 1

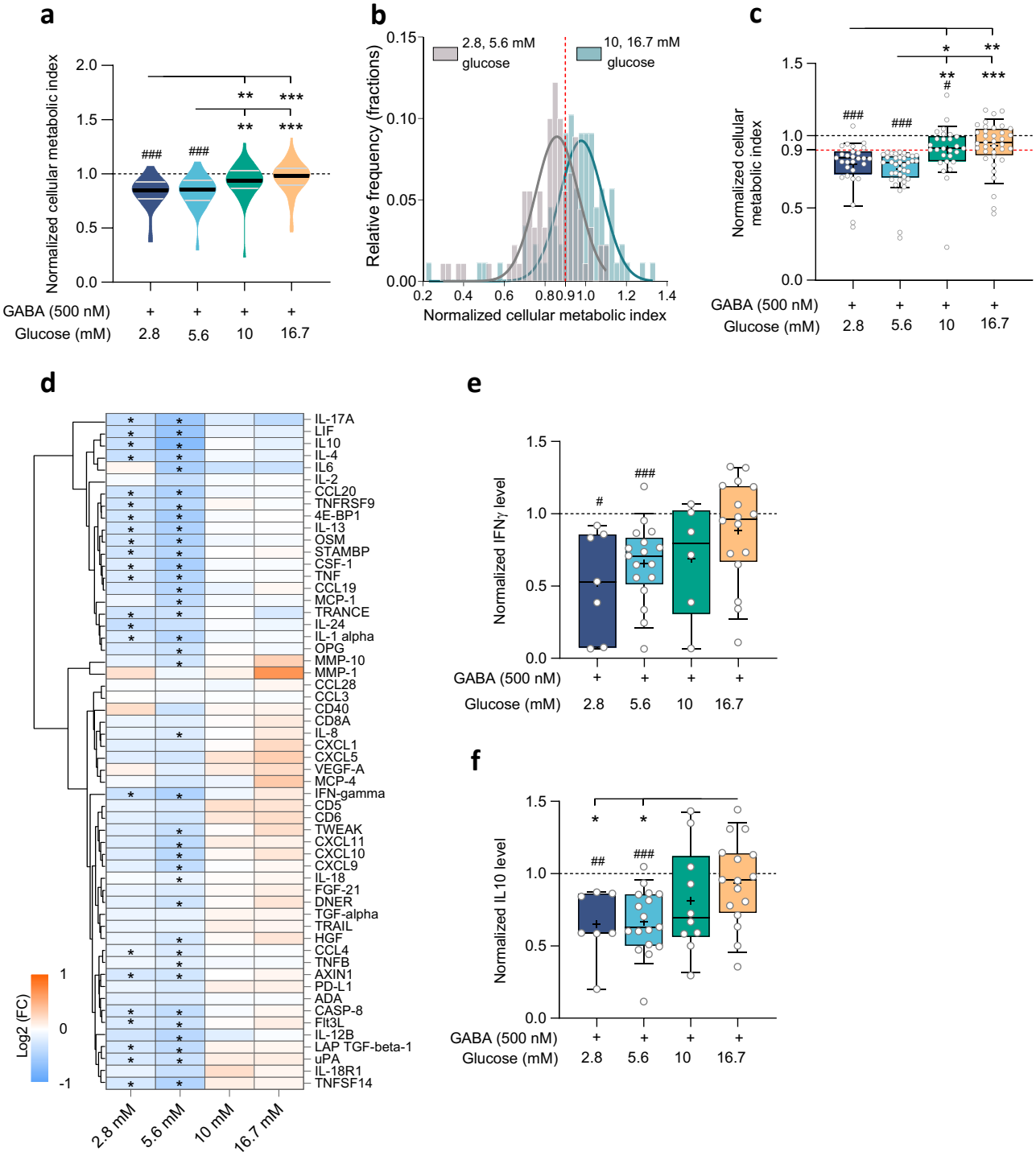
a
Normalized cellular metabolic index
GABA (500 nM)
Glucose (mM)
2.8
5.6
10
16.7
b
2.8, 5.6 mM glucose
10, 16.7 mM glucose
Relative frequency (fractions)
Normalized cellular metabolic index
c
Normalized cellular metabolic index
d
IL-17A
LIF
IL10
IL-4
IL6
IL-2
CCL20
TNFRSF9
4E-BP1
IL-13
OSM
STAMBP
CSF-1
TNF
CCL19
MCP-1
TRANCE
IL-24
IL-1 alpha
OPG
MMP-10
MMP-1
CCL28
CCL3
CD40
CD8A
IL-8
CXCL1
CXCL5
VEGF-A
MCP-4
IFN-gamma
CD5
CD6
TWEAK
CXCL11
CXCL10
CXCL9
IL-18
FGF-21
DNER
TGF-alpha
TRAIL
HGF
CCL4
TNFB
AXIN1
PD-L1
ADA
CASP-8
Flt3L
IL-12B
LAP TGF-beta-1
uPA
IL-18R1
TNFSF14
Log2 (FC)
2.8 mM
5.6 mM
10 mM
16.7 mM
e
Normalized IFNγ level
f
Normalized IL10 level

Figure 1. GABA effects on metabolic activity and cytokine release are glucose concentration-dependent in activated $CD4^+$ T cells.

a, Violin plots show cellular metabolic activity of activated $CD4^+$ T cells as measured by MTT assay, in the presence of GABA at different glucose concentrations: 2.8 (N=36), 5.6 (N=54), 10 (N=35) and 16.7 mM (N=53). Horizontal black and grey lines indicate the median and quartiles, respectively.

b, Distribution (histogram and Gaussian fit) of normalized cellular metabolic activity of $CD4^+$ T cells at low-normal (2.8 and 5.6 mM) and high (10 and 16.7 mM) glucose concentrations. Solid lines: Gaussian fits, vertical broken line: 10% inhibition by GABA (500 nM). X-axis: normalized cellular metabolic index, Y-axis: relative frequency represented as fractions.

c, Box plots show metabolic activity of activated $CD4^+$ T cells from donors where $\geq$10% GABA inhibition was observed at 5.6 mM glucose; 2.8 (N=28), 5.6 (N=37), 10 (N=27) and 16.7 (N=36).

d, Heatmap and hierarchical clustering of inflammatory-related biomolecules by PEA 72 h post-stimulation of $CD4^+$ T cells, at different glucose concentrations (N=17). Data represent the mean log2 (fold change) for samples cultured in presence and compared to absence of GABA.

e, f, Box plots show GABA inhibition of IFNγ **(e)** and IL-10 **(f)** release, as measured by ELISA, glucose concentrations (mM): 2.8 (N=7;7), 5.6 (N=17;17), 10 (N=6;10) and 16.7 (N=16;16) in **e** and **f**, respectively.

Data were normalized to values of activated cells in the absence of drugs at each glucose concentration (**a, c, e, f**). Box and whisker (**c, e, f**): 10-90 percentiles, means: +, medians: black lines in the boxes. Statistics: one sample t-test when compared to activated cell group (#, $p < 0.05$; ##, $p < 0.01$; ###, $p < 0.001$), paired groups by repeated measures ANOVA or fitting a mixed-effects model, or ordinary one-way ANOVA followed by Tukey (**a, c, e, f**) for multiple comparisons (*, $p < 0.05$; **, $p < 0.01$; ***, $p < 0.001$). Statistical significance in **d** (**(**$p \leq 0.05$ and adjusted p-value $q < 0.12$) are marked with *. **N**: donors.

Figure 2

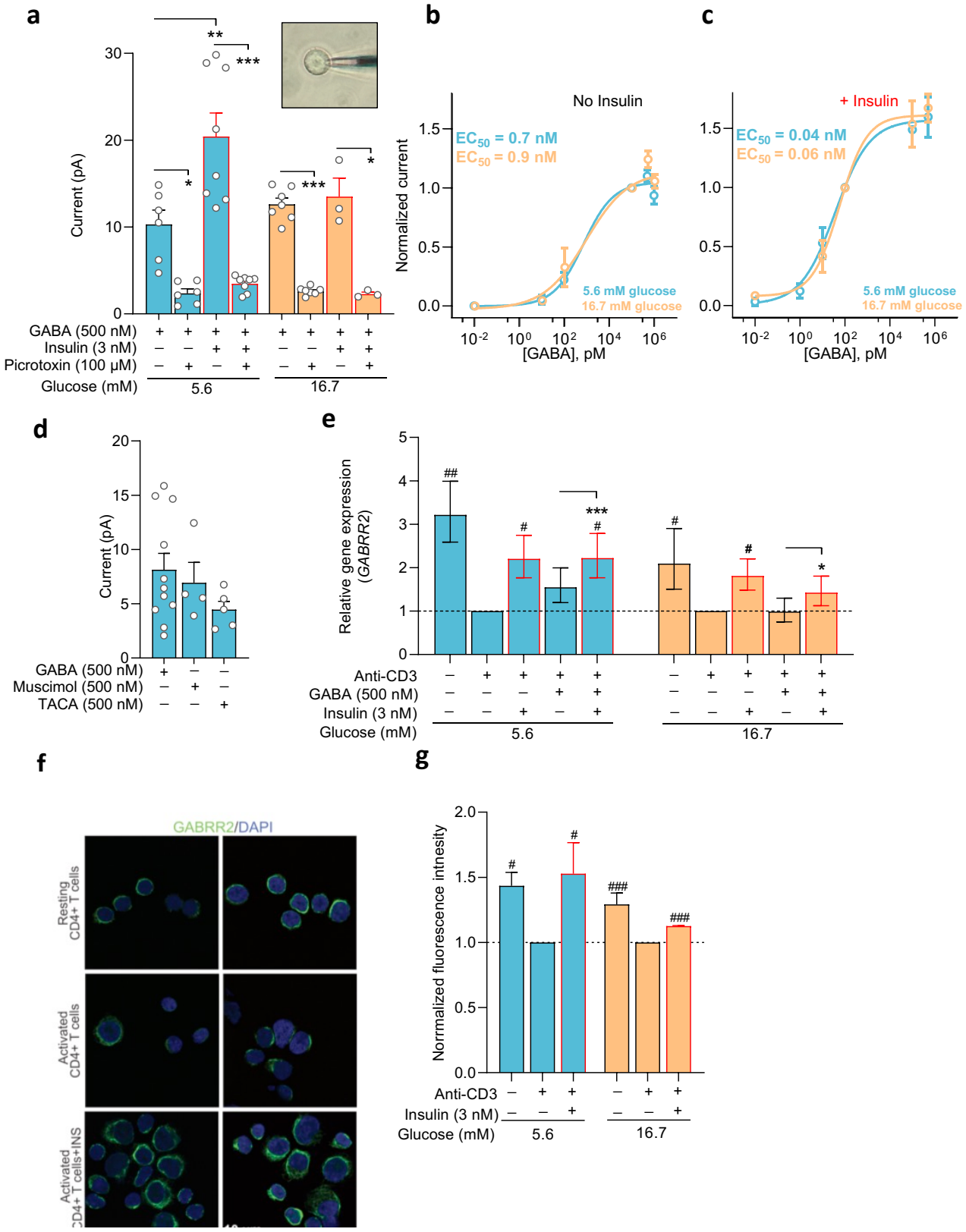
a
Current (pA)
GABA (500 nM)
Insulin (3 nM)
Picrotoxin (100 μM)
Glucose (mM)
5.6
16.7
b
No Insulin
Normalized current
EC50 = 0.7 nM
EC50 = 0.9 nM
5.6 mM glucose
16.7 mM glucose
[GABA], pM
c
+ Insulin
EC50 = 0.04 nM
EC50 = 0.06 nM
5.6 mM glucose
16.7 mM glucose
[GABA], pM
d
Current (pA)
GABA (500 nM)
Muscimol (500 nM)
TACA (500 nM)
e
Relative gene expression (GABRR2)
Anti-CD3
GABA (500 nM)
Insulin (3 nM)
Glucose (mM)
5.6
16.7
f
GABRR2/DAPI
Resting CD4+ T cells
Activated CD4+ T cells
Activated CD4+ T cells+INS
g
Norrmalized fluorescence intnesity
Anti-CD3
Insulin (3 nM)
Glucose (mM)
5.6
16.7

461 **Figure 2. Insulin enhances GABA-activated $GABA_AR$ currents and regulates $GABA_A$ receptor**
462 **expression in activated $CD4^+$ T cells.**
463 **a,** GABA-activated whole-cell currents (at +30 mV) in the absence or presence of a $GABA_AR$
464 antagonist picrotoxin (PTX) in activated $CD4^+$ T cells without or treated with insulin (n=3-8,
465 N=11). Insert: a patch-pipette attached to an activated $CD4^+$ T cell.
466 **b, c,** GABA dose-response curves and the calculated half maximal effective concentration
467 (EC_{50}) in cells without (**b**) or treated with (**c**) insulin. The currents were normalized to 100 nM
468 (**b**) or 100 pM (**c**) GABA responses (n=3–11, N=27).
469 **d,** Whole-cell currents (at +30 mV) evoked by $GABA_AR$ agonists GABA (n=11, N=9), muscimol
470 (n=4, N=3) or TACA (n=5, N=4), in activated $CD4^+$ T cells in 5.6 mM glucose.
471 **e,** Relative expression of *GABRR2* mRNA in resting and anti-CD3 antibody-activated cells in 5.6
472 or 16.7 mM glucose (N=6) analyzed by $2^{-\Delta\Delta Ct}$ method.
473 **f,** Representative images from immunofluorescence co-staining of GABRR2 (green) and DAPI
474 (blue) in $CD4^+$ T cells in 5.6 or 16.7 mM glucose.
475 **g,** Bar graphs show quantification of GABRR2 fluorescence intensity in $CD4^+$ T cells (n>50
476 cells/group, N=3).
477 Data represent mean ± SEM in (**a, d, g**) and geometric mean ± SEM in (**e**). Data were normalized
478 to values of activated cells in the absence of drugs at each glucose concentration (**e, g**). Curve
479 fitting (**b, c**): nonlinear regression with sigmoidal polynomial (4PL) model. Statistics: ordinary
480 one-way ANOVA followed by Tukey (**a, d, g**) or repeated measures ANOVA followed by Fisher's
481 LSD test (**e**) for multiple comparisons. (*, $p < 0.05$; **, $p < 0.01$; ***, $p < 0.001$. #, $p < 0.05$; ###,
482 $p < 0.001$when compared to activated cell group). **n**: cells, **N**: donors.
483
484
485
486

Figure 3

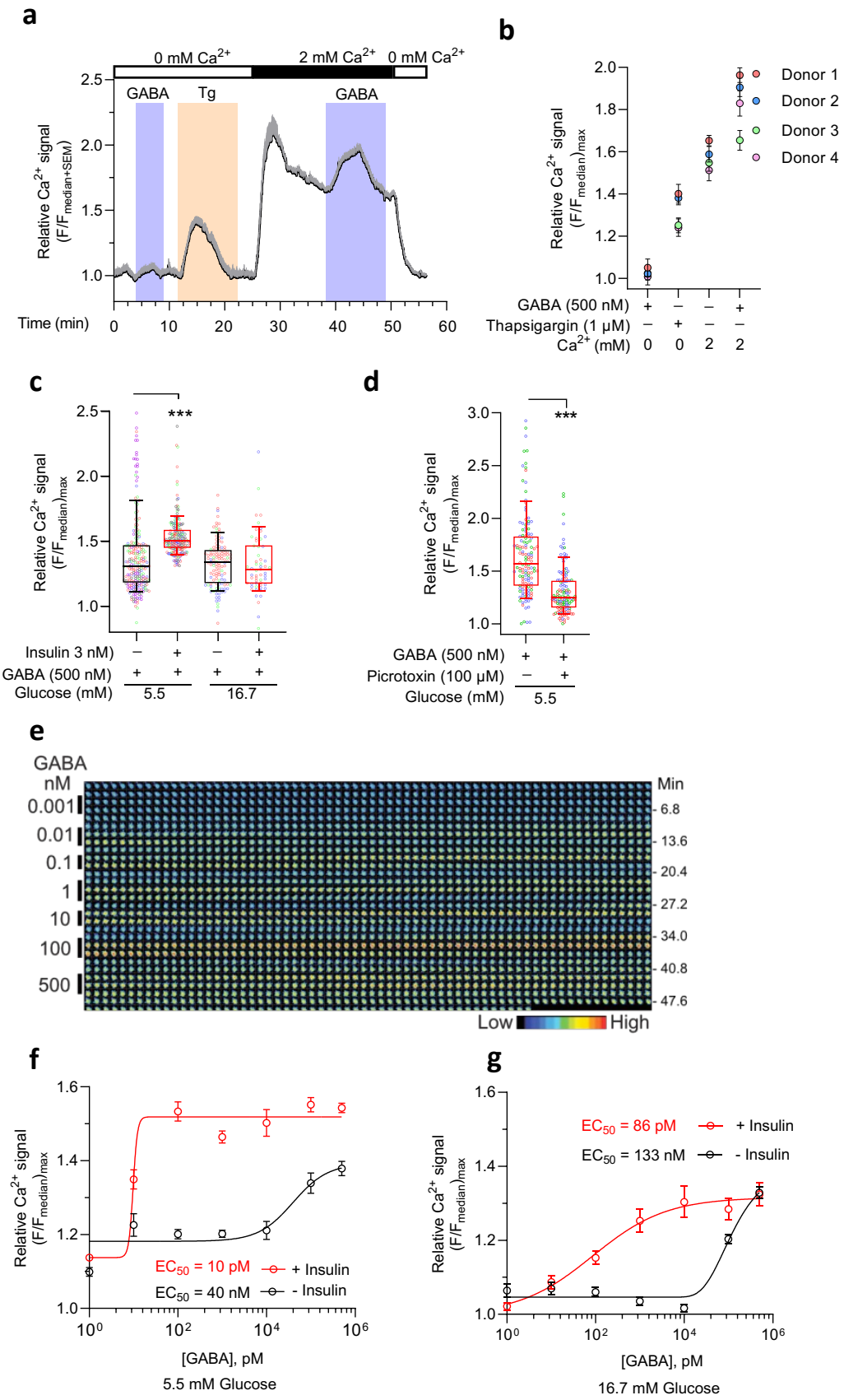
a
0 mM Ca2+
2 mM Ca2+
0 mM Ca2+
GABA
Tg
GABA
Relative Ca2+ signal (F/Fmedian+SEM)
Time (min)
b
Donor 1
Donor 2
Donor 3
Donor 4
Relative Ca2+ signal (F/Fmedian)max
GABA (500 nM)
Thapsigargin (1 μM)
Ca2+ (mM)
c
***
Insulin 3 nM)
GABA (500 nM)
Glucose (mM)
5.5
16.7
d
***
GABA (500 nM)
Picrotoxin (100 μM)
Glucose (mM)
5.5
e
GABA nM
Min
Low
High
f
EC50 = 10 pM
+ Insulin
EC50 = 40 nM
- Insulin
[GABA], pM
5.5 mM Glucose
g
EC50 = 86 pM
+ Insulin
EC50 = 133 nM
- Insulin
[GABA], pM
16.7 mM Glucose

Figure 3. Insulin elevates GABA-activated Ca^{2+} entry in human $CD4^+$ T cells.

a, Mean Ca^{2+} signal intensity trace (black line) and SEM (gray whiskers) recorded 72 h after activation of cells (n=14). Colored bars: Perfusion time of drugs (GABA 500 nM and thapsigargin, Tg 1 µM) in 0 or 2 mM Ca^{2+}-containing perfusion medium.

b, Relative Ca^{2+} signal (mean ± SD) recorded in activated $CD4^+$ T cells (n=14, 20, 41, 47, N= 4).

c, GABA-activated relative Ca^{2+} signal recorded in activated $CD4^+$ T cells (n=58-232, N=3-5) without or treated with insulin.

d, GABA-activated relative Ca^{2+} signal in activated $CD4^+$ T cells (n=131, N=3) in absence or presence of picrotoxin, with insulin.

e, Representative time-lapsed micrographs of a live Ca^{2+} imaged cell (16.7 mM glucose, with insulin). GABA concentrations (vertical bars on the left) were sequentially perfused (time indicated as min on the right) and inter-spaced with medium applications. Color scale: Relative Ca^{2+} fluorescence intensity.

f, g, Dose-response relationship and the calculated half maximal effective GABA concentration (EC_{50}) for GABA-induced Ca^{2+} signals in activated $CD4^+$ T cells without or treated with insulin in 5.5 mM (**f**) or 16.7 mM (**g**) glucose (n=63-279, N=3-8), see also Supplementary Figure 3e.

In (**c, d**), individual data point represents relative Ca^{2+} signal recorded from each cell and is color-coded based on donors and box-whisker plots display the 10-90 percentile at the whiskers. Statistics: Two-tailed unpaired (**c**) or paired (**d**) Student's t-test, ***, $p < 0.001$. **n**: cells, **N**: donors.

Figure 4

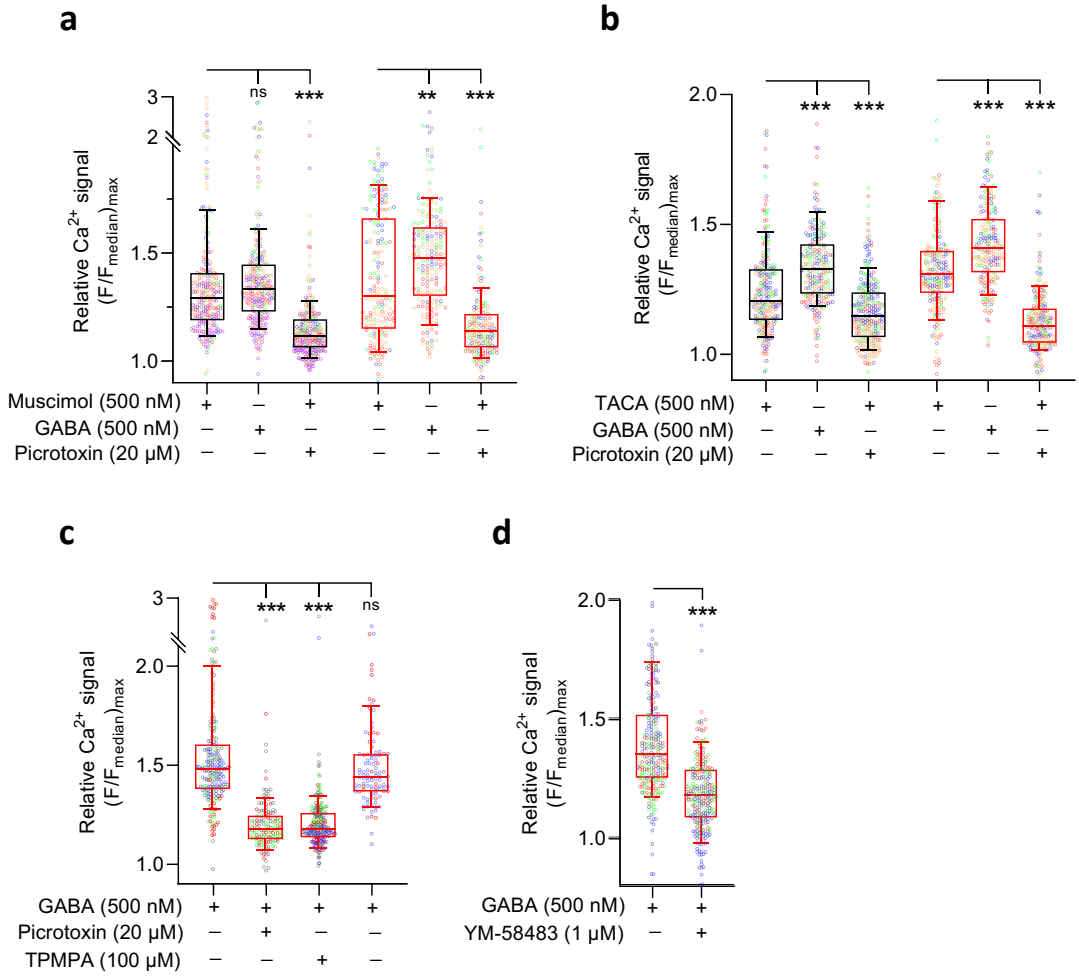

Figure 4. Pharmacological modulation of GABA-activated Ca^{2+} entry in human $CD4^+$ T cells
Effects of $GABA_AR$ agonist, muscimol (500 nM, **a**) and TACA (500 nM, **b**), $GABA_AR$ antagonist picrotoxin (PTX, 20 µM, **a, b, c**) and TPMPA (100 µM, **c**), and SOCE antagonist YM48583 (1 µM, **d**) on relative Ca^{2+} signal in activated $CD4^+$ T cells in 5.5 mM glucose (n=191-265, N=3-5).

Individual data point represents relative Ca^{2+} signal recorded from each cell and is color-coded based on donors. Box-whisker plots (black without and red with insulin) display the 10-90 percentile at the whiskers. Statistics: repeated measures ANOVA followed by Tukey multiple comparison test (**a, b, c**) or two-tailed paired (**d**) Student's t-test. ns, $p > 0.05$, **, $p < 0.01$, ***, $p < 0.001$. **n**: cells, **N**: donors.

Figure 5

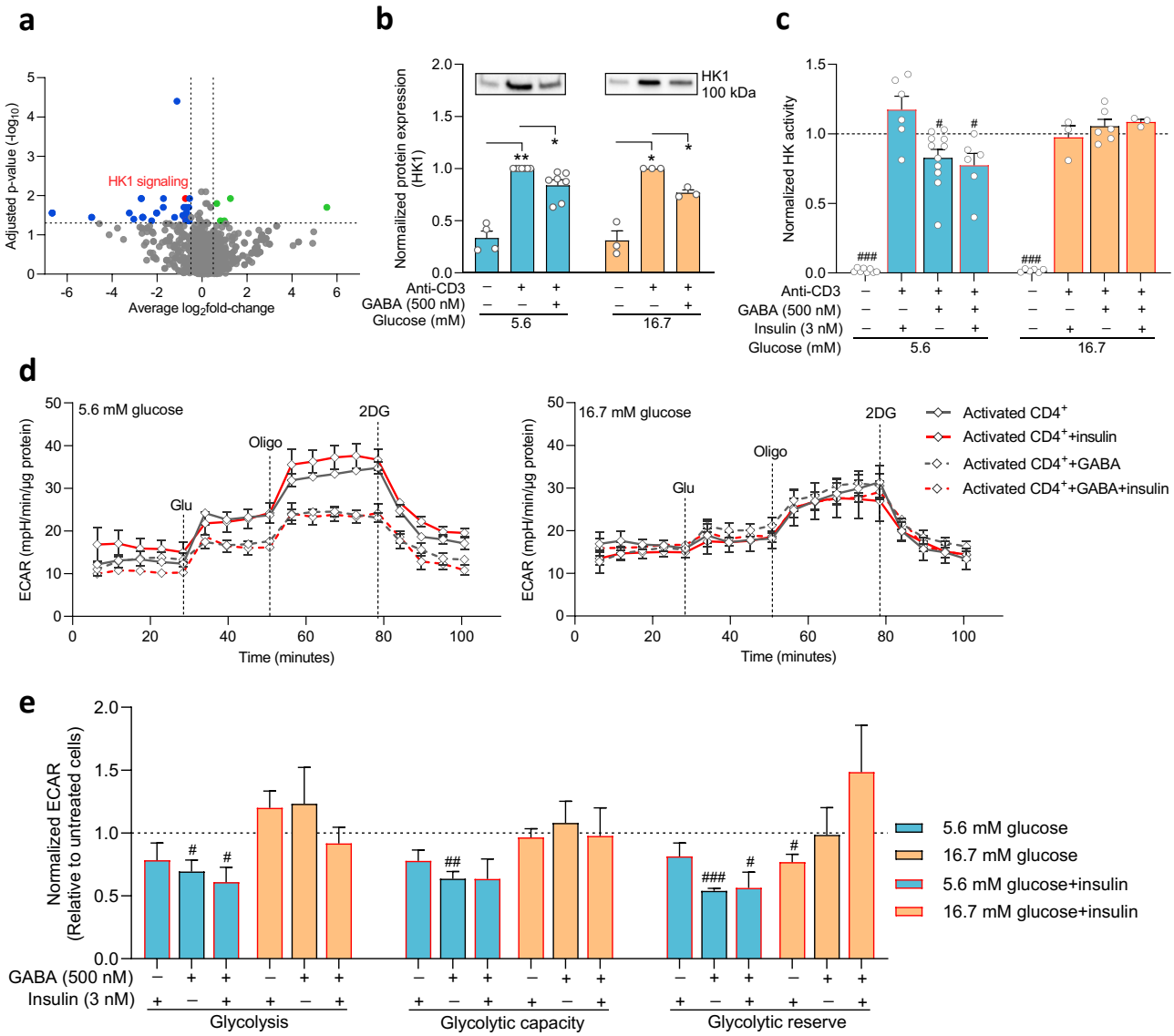

Figure 5. GABA inhibits hexokinase and glycolysis in activated CD4⁺ T cells.
a, The volcano plot summarizes pathways that are significantly up- (green) or down-regulated (blue and red (HK1)) by GABA treatment in cells 72 h post activation (N=5), 5.6 mM glucose. The x-axis represents the average fold-change of all proteins measured by mass spectrometry within that pathway and every dot is one pathway. The y-axis represents the adjusted p-value (-log10 transformation). The horizontal line represents p = 0.05, and the vertical lines represent average log2 (fold change) < -0.5 or > 0.5.
b, Western blot images and relative expression of HK1 protein (N=3-7).
c, *In vitro* HK activity analyzed in resting and activated cells, 5.6 mM (N=12) or 16.7 mM (N=6) glucose. HK activity (µmol NADH/min/ml) was normalized to the activity of activated cells in the absence of drugs.
d, Representative ECAR over time in cells 72 h post-activation treated with or without GABA (500 nM) or insulin at 5.6 mM (left panel) or 16.7 mM (right panel). Dashed lines indicate injections into media of glucose (Glu.), oligomycin (Oligo) or 2-deoxyglucose (2-DG).

e. ECAR results (mpH/min/protein) were normalized to controls in absence of drugs for average glycolysis, glycolytic capacity and glycolytic reserve in cells 72 h post-activation treated with or without GABA or insulin, 5.6 mM (N=5) or 16.7 mM (N=5) glucose.

Data are normalized to values of activated cells in the absence of drugs at each glucose concentration (**b, c, e**). Data represent mean ± SEM (**b, c, d, e**). Statistics: one sample t-test when compared to activated cell group (#, $p < 0.05$; ##, $p < 0.01$; ###, $p < 0.001$), repeated measures ANOVA or fitting a mixed-effects model followed by Tukey multiple comparison test. **N**: donors.

Figure 6

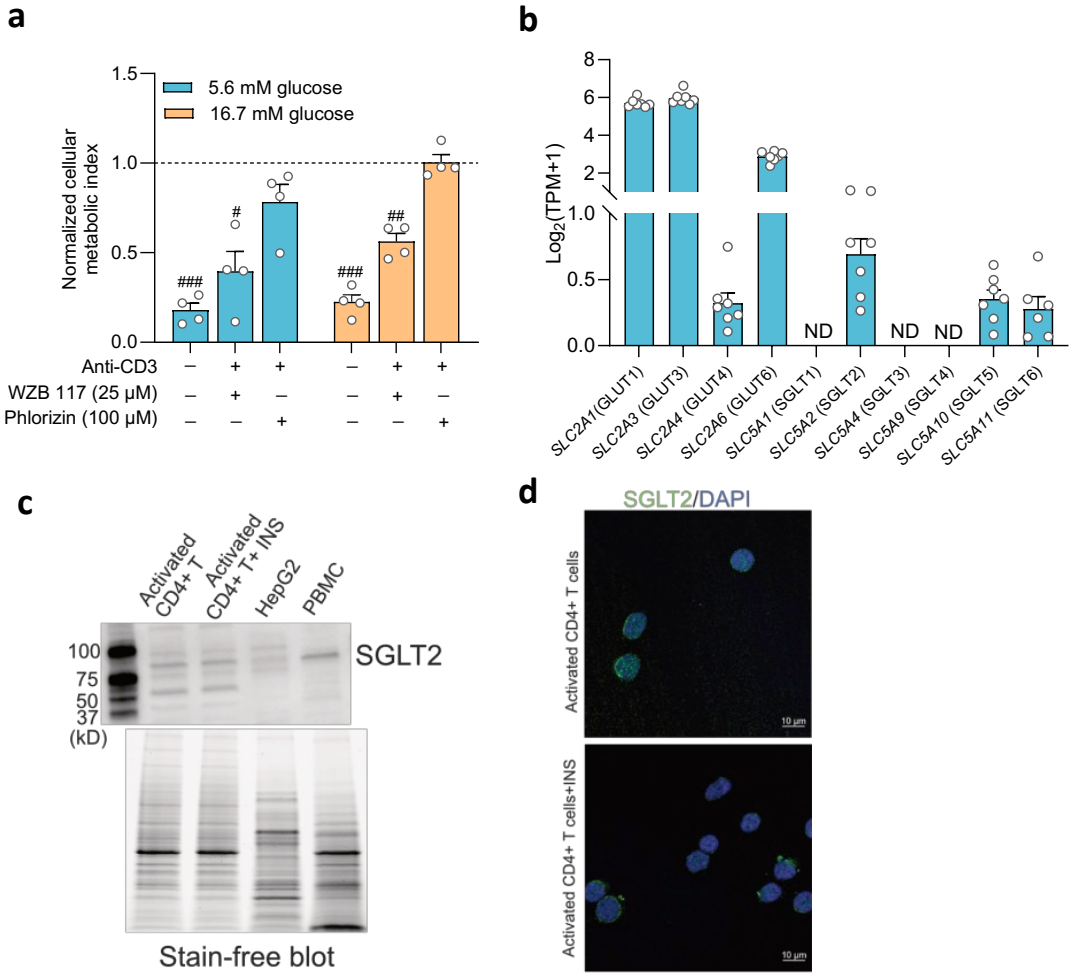

Figure 6. Sodium-glucose co-transporter 2 (SGLT2) is expressed in activated human CD4⁺ T cell.

a, The cellular metabolic activity of resting and activated cells in presence of GLUT1 inhibitor, WZB 117 or SGLTs inhibitor, phlorizin was normalized to that of activated cells without drug treatment in 5.6 mM or 16.7 mM glucose (N=4). Data represent mean ± SEM. Statistics: one sample t-test when compared to activated cell group (#, $p < 0.05$; ##, $p < 0.01$; ###, $p < 0.001$)

b, Relative gene expression levels of facilitated glucose transporters (GLUTs) and Na^+-dependent glucose transporters (SGLTs) in activated cells at 5.6 mM glucose (N=6) determined by RNAseq analysis. TPM, transcripts per million. Data represent mean ± SEM. ND, not detected.

c, Representative Western blot image of SGLT2 protein in activated $CD4^+$ T cells and HEPG2 cell line. The stain-free blot image represents total proteins loaded for each sample, insulin (INS, 3 nM), 16.7 mM glucose.

d, Representative immunofluorescence co-staining of SGLT2 (green) and DAPI (blue) in $CD4^+$ T cells, 5.6 mM or 16.7 mM glucose.

N: donors.

Figure 7

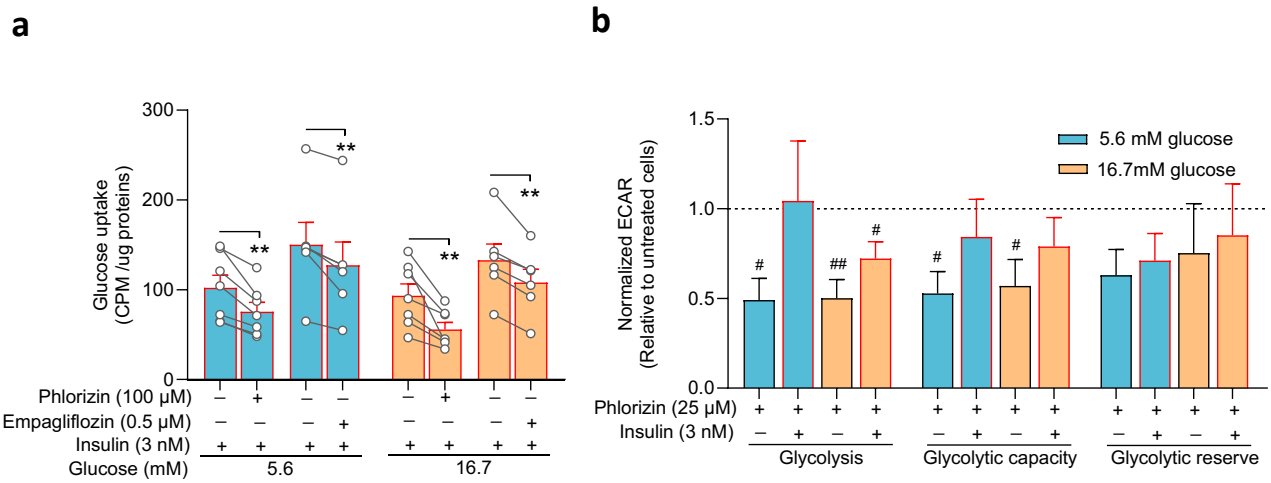

Figure 7. SGLT2 is functional and modulates glycolysis in activated human CD4$^+$ T cell.
a, Glucose uptake in absence or presence of phlorizin (N=7) and SGLT2 selective inhibitor, empagliflozin (N=6) in cells 72 h post-activation, with insulin, in 5.6 mM or 16.7 mM glucose. Data represent before and after inhibitor treatment from each donor as well as mean ± SEM. Statistics: two-tailed paired Student's t-test, *, $p < 0.05$. CPM: count per minute.
b, Extracellular acidification rate (ECAR) results (mpH/min/protein) normalized to activated cells in the absence of drugs for average glycolysis, glycolytic capacity and glycolytic reserve in cells, 72 h post-activation, incubated with phlorizin, with or without insulin in 5.6 mM (N=5) or 16.7 mM (N=5) glucose. Data represent mean ± SEM. Statistics: one sample t-test (#, $p < 0.05$; ##, $p < 0.01$).
N: donors.

Figure 8

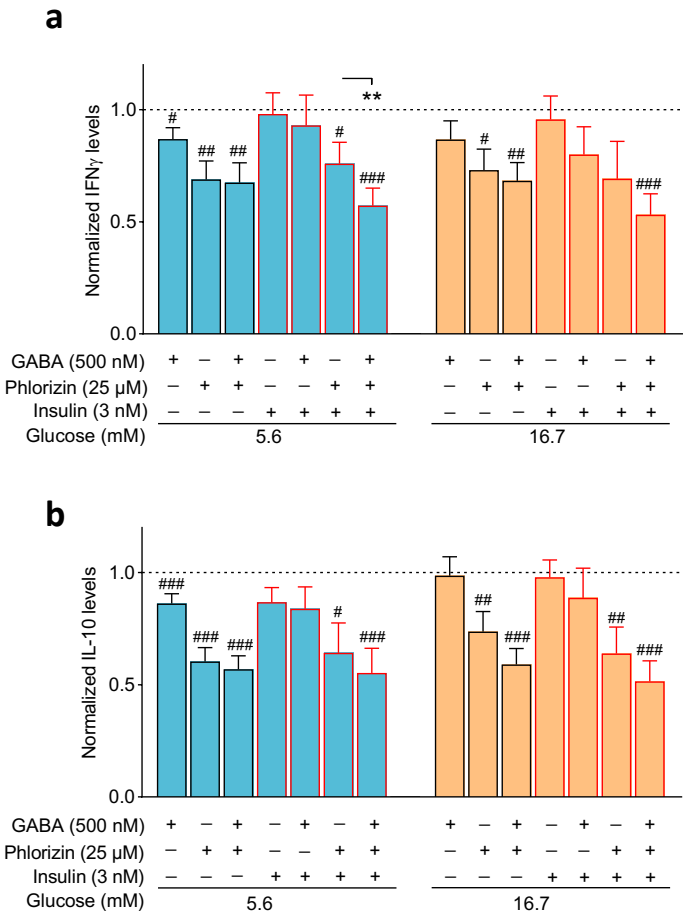

Figure 8. SGLT2 modulates cytokine release in activated human CD4⁺ T cell.
Bar graphs show IFNγ **(a)** and IL-10 **(b)** release from activated cells 72 h post-activation in with or without GABA, phlorizin or insulin, at 5.6 mM or 16.7 mM glucose (N=17). Data represent mean ± SEM. Data are normalized to values of activated cells in the absence of drugs at each glucose concentration. Statistics: one sample t-test when compared to activated cell group (#, $p < 0.05$; ##, $p < 0.01$; ###, $p < 0.001$), repeated measure one-way ANOVA or Mixed-effects analysis with Tukey multiple comparisons, **, $p<0.01$. **N**: donors.

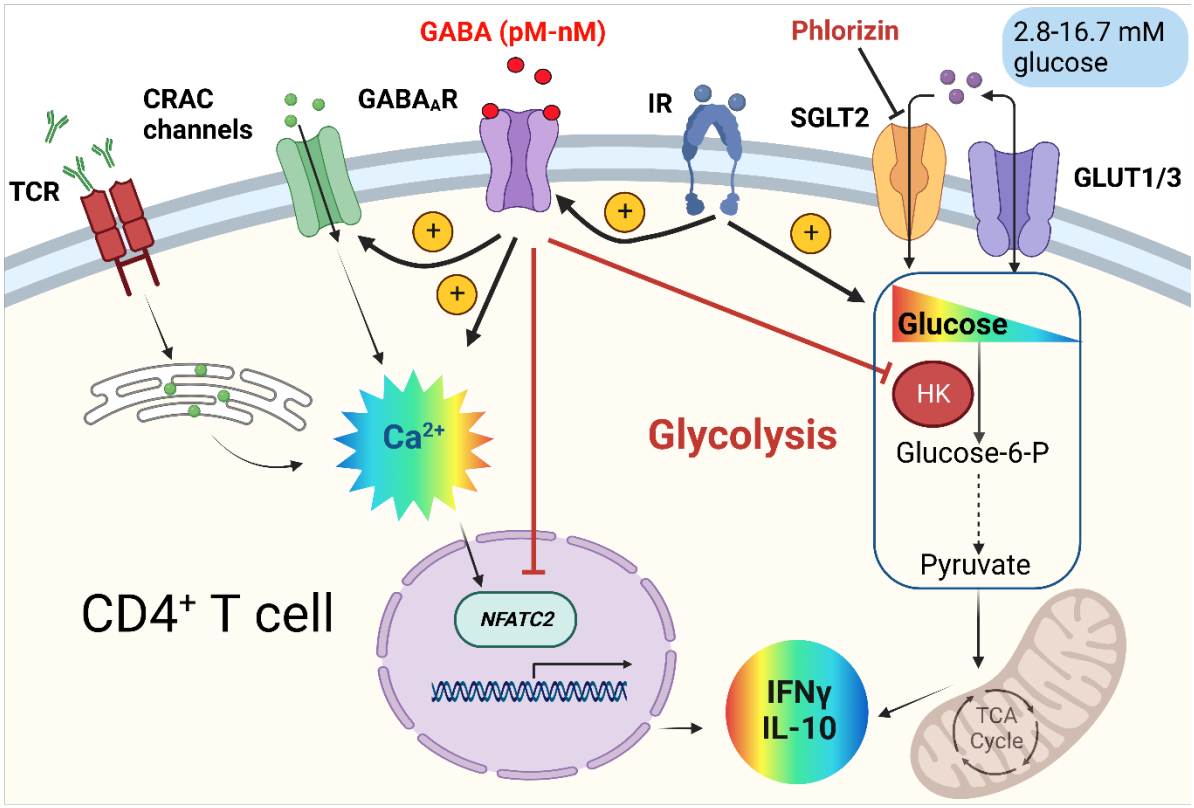

Figure 9. GABA, glucose and insulin regulate CD4+ T cell effector functions.
In human CD4+ T cells, the activation of T cell receptor (TCR)/CD3 complex by anti-CD3 antibodies binding, initiates store-operated Ca2+ entry (SOCE) through Ca2+ release-activated Ca2+ (CRAC) channels. It regulates intracellular Ca2+ signals, drives changes in transcription factors, upregulates glycolysis and increases T cell effector functions. Physiological concentration of GABA (pM-nM) activates GABAA receptors (GABAAR) to modulate T cells metabolic activity and levels of cytokines (e.g., IFNγ and IL-10) by 1) enhancing function of CRAC channels and Ca2+ entry; 2) reducing expression of Nuclear Factor of Activated T cell 2 (NFATC2 or NFAT1); 3) decreasing expression and activity of hexokinase (HK), the 1st rate-limiting enzyme in aerobic glycolysis. In addition, insulin-insulin receptor (IR) signaling promotes glycolysis but paradoxically reduce glycolysis by enhancing GABAAR function. The fluctuation of blood glucose concentration affects glycolysis and cytokine production. Glucose uptake is mediated by not only the facilitated glucose transporters GLUT1/3 but also the sodium-dependent glucose transporter 2 (SGLT2). Phlorizin, a SGLT inhibitor, reduces glucose uptake, attenuates glycolysis and reduces IFNγ and IL-10 levels.
Created with BioRender.com.

Supplementary information

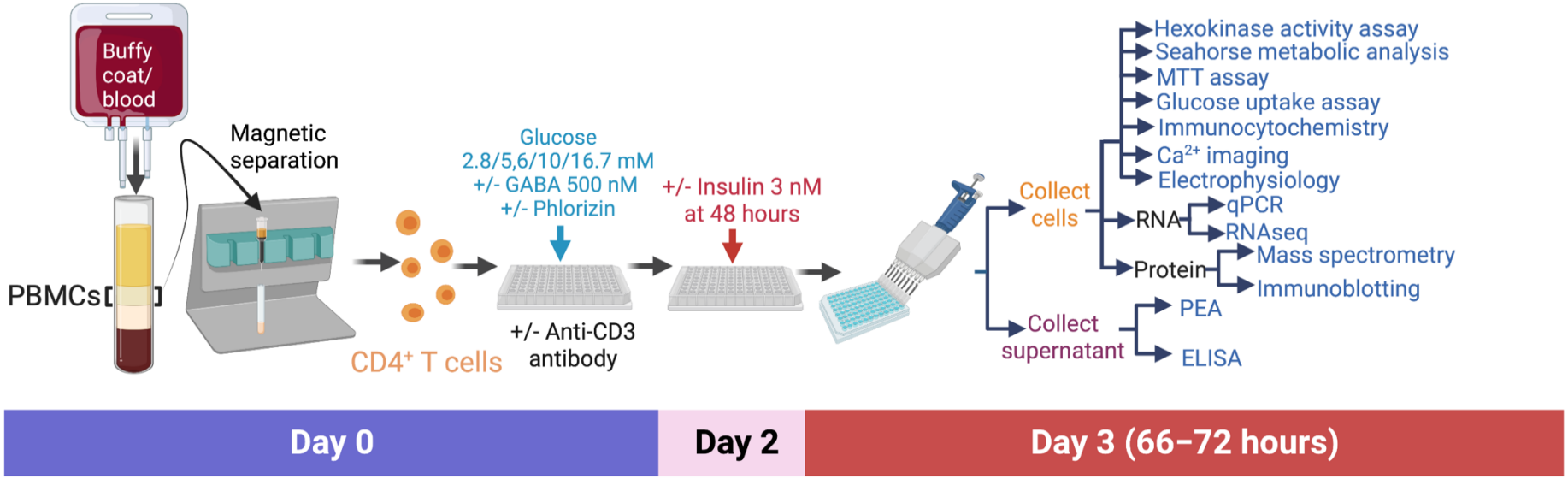

Supplementary Fig. 1: Schematic diagram of the experimental design.
Created with BioRender.com.

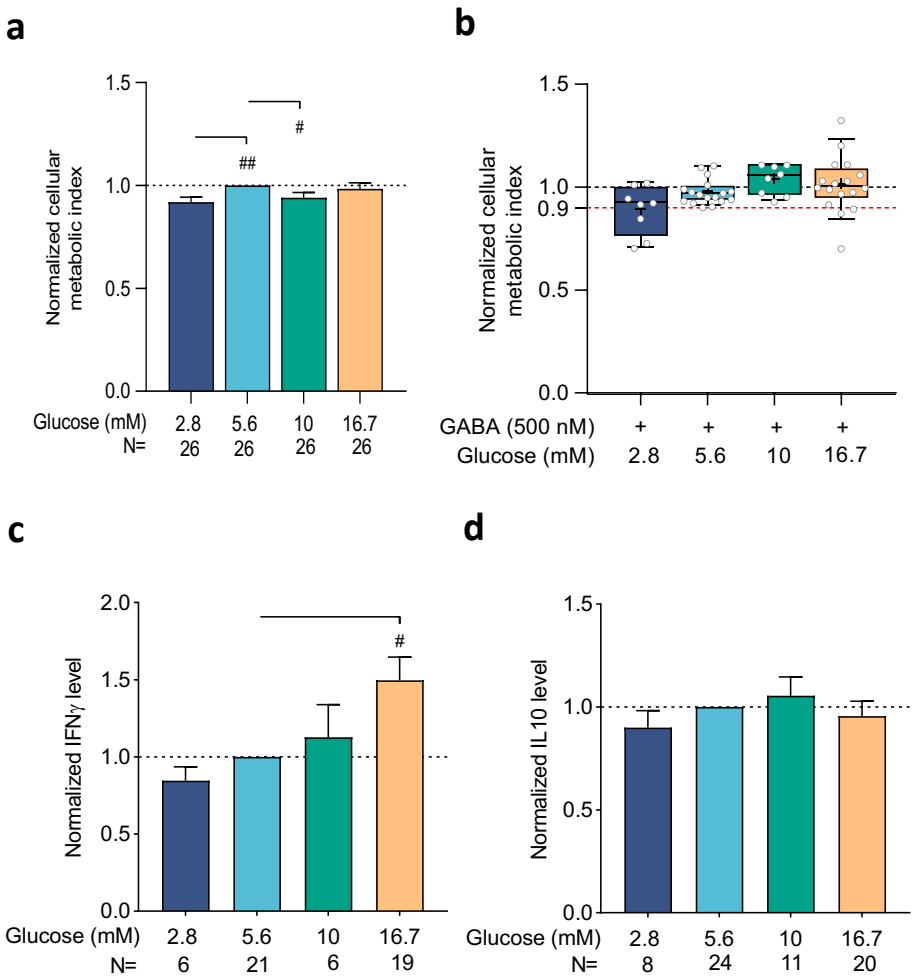

Supplementary Fig. 2: The effect of glucose on cellular metabolic activity and release of IFNγ and IL-10 from CD4⁺ T cells.

a, Cellular metabolic activity of CD4⁺ T cells 72 h after activation in the presence of different glucose concentrations. **b,** Cellular metabolic activity from donors where <10% GABA inhibition at 5.6 mM glucose was observed. **c, d,** IFNγ (**c**) and IL-10 (**d**) released from CD4⁺ T cells 72 h after activation in presence of different glucose concentrations. Data are normalized to values at 5.6 mM glucose and presented as mean ± SEM. Statistics by one sample t-test when compared to 5.6 mM glucose group (#, $p < 0.05$; ##, $p < 0.01$), repeated measures ANOVA or fitting a mixed-effects model followed by Tukey test for multiple comparisons. N: donors.

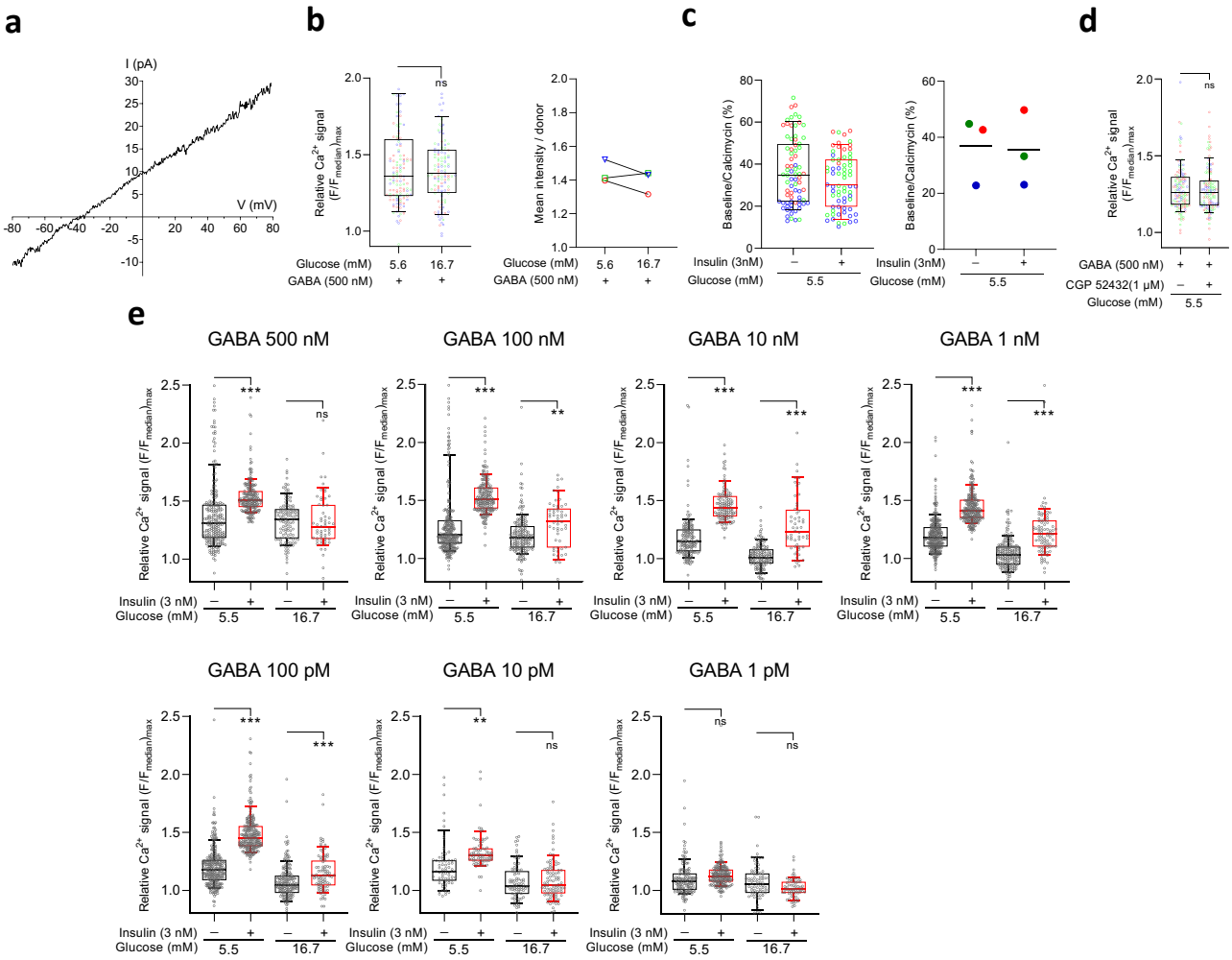

Supplementary Fig. 3: GABA-activated current and Ca^{2+} signaling in $CD4^+$ T cells.
a, A representative current-voltage relationship recorded in an activated $CD4^+$ T cell in response to 500 nM GABA application by perforated patch-clamp, 5.6 mM glucose. **b,** GABA (500 nM)-activated relative Ca^{2+} signals (left panel) and mean intensity (right panel) recorded from activated $CD4^+$ T cells (n=128 cells/ N=3 donors) in sequentially applied 5.6 mM and 16.7 mM glucose-containing media. Cells were activated in 5.5 mM glucose-containing media for 72 hours. **c,** The ratio of Ca^{2+} signals in the absence and presence of calcium-ionophore calcimycin (1 µM) in $CD4^+$ T cells (n=85 cells left panel/ N=4 donors right panel) 72 h after activation with or without insulin treatment. **d,** GABA-activated relative Ca^{2+} signal recorded in $CD4^+$ T cells (n=131 cells/ N=3 donors) in the absence or presence of $GABA_B$ receptor antagonist CGP 52432 (1 µM) at 5.5 mM glucose. **e,** Relative Ca^{2+} signals induced by different concentrations of GABA in activated $CD4^+$ T cells treated without or with insulin in 5.5 mM or 16.7 mM glucose. Statistics by two-tailed student's t-test. ns, $p > 0.05$, **, $p < 0.01$; ***, $p < 0.001$.

42 **Supplementary Table 1 | Donors' demographic information**

Parameter	Normal Donors (N=160)
Age (years)	26.2 ± 0.25
Sex (N, %)	89 males (55.6%)
	71 females (44.4%)

43
44 Data are presented as means ± SEM.
45
46
47
48
49
50
51

52
53
54
55
56
57
58
59
60
61

Supplementary Table 2 I Relative gene quantification (normalized to activated cells) by qPCR (N=7-11 donors).

Gene name	5.6 mM glucose					16.7 mM glucose				
	Resting	Activated	Activated+Insulin	GABA	GABA+Insulin	Resting	Activated	Activated+Insulin	GABA	GABA+Insulin
NFATC1	0.088	1***	1.129***	1.086**	1.140***	1.902	1**	1.017	1.072*	0.923**
NFATC2	0.996	1	0.980	0.884$^{\#\#}$	0.942	1.333	1	0.961$^{\&}$	1.121	0.876$^{*, \&}$
NFATC3	0.512	1**	0.929**	0.836*	0.773**	0.484	1*	0.895$^{*, \&}$	1.057**	0.922*
JAK1	1.808	1***	1.156	1.096***	1.144$^{***, \#}$	2.123	1	1.049	1.329	1.027
JAK2	0.405	1***	1.060***	1.085***	1.133***	0.291	1	0.802	1.041	0.932
TYK2	1.639$^{\#}$	1	1.278	1.016	0.997*	1.254	1	0.716	0.826	0.596
HIF1A	0.310	1***	1.005***	0.961***	0.960***	0,287	1***	0.919***	0.968***	0.794***
STAT1	0.088	1***	1.129$^{***, \#}$	1.086***	1.140***	0.067	1***	0.939***	0.925***	0.981***
MYC	0.626	1**	0.925**	0.918*	0.946**	0.368	1**	0.662$^{\#}$	0.805*	0.787*

*p<0.05, **p<0.01, ***p<0.001, as compared to resting cells; #p<0.05, ##p<0.01, as compared to activated cells: &p<0.05, as compared to GABA-treated cells. The statistical analysis was performed on ΔCq values with repeated measures one-way ANOVA with Fisher's LSD test for multiple comparison.

Supplementary Table 3 | Reactome analysis of MS data (N=5 at 5.6 mM glucose). Proteins are named after UniProtKB.

Top up-regulated proteins

Identifier	logFC	AveExpr	t	P.Value
K2C79_HUMAN	0.67266061	13.2926208	2.34394122	0.04308325
CHM4A_HUMAN	0.55827697	13.7149206	2.20925349	0.05380739
HLAH_HUMAN	1.03346983	14.8113954	2.03947592	0.07106636
RAB2A_HUMAN	1.37200668	14.1750267	2.03797883	0.07123998
SC11A_HUMAN	5.70132617	10.587487	1.91122932	0.08749562
K22O_HUMAN	0.48972535	12.2546633	1.88242372	0.09164997
DYL1_HUMAN	5.54957599	10.7818438	1.81112175	0.10274055
PLXA4_HUMAN	0.69449352	13.706242	1.7195177	0.11881622
RL36_HUMAN	6.02123532	12.32297	1.68555819	0.12534011
IF4G2_HUMAN	0.82748497	13.4787932	1.68221061	0.12600056

Top down-regulated proteins

Identifier	logFC	AveExpr	t	P.Value
TBB1_HUMAN	-7.55965074	8.58464831	-2.74841088	0.02204275
STA5B_HUMAN	-7.60692039	6.04448902	-2.44305026	0.03656351
EXOS3_HUMAN	-6.6014009	5.67159622	-2.16624065	0.05775108
BGAL_HUMAN	-6.67048214	5.77846898	-2.13711593	0.06057899
AL1B1_HUMAN	-6.67577438	5.87276979	-2.08793829	0.06566002
HXK1_HUMAN	-0.73989819	14.3697968	-2.06803575	0.06783079
HLAG_HUMAN	-6.34860408	5.64345434	-2.03980339	0.07102844
COPG1_HUMAN	-5.15586276	10.0461233	-1.80136877	0.10435116
BCL2_HUMAN	-4.91388319	9.86964223	-1.73134501	0.11661798
PIP_HUMAN	-4.68190741	9.67505331	-1.66669489	0.12910318

Methods

Study individuals and collection of samples

Human blood buffy coat and blood samples were obtained from Uppsala University Hospital (Uppsala Akademiska sjukhuset), protocol approved by the Regional Research Ethical Committee in Uppsala. All donors were voluntary recruited and informed consent were signed. In total, samples from 160 normal donors, 89 men and 71 women with mean age 26.2 ± 0.25 years were included in the study.

Chemicals and reagents

Drugs, buffers and salts unless otherwise specified were purchased from Sigma-Aldrich/Merck (Steinheim, Germany). TACA, muscimol, TPMPA, YM-58483, WZB 117 were purchased from Tocris (UK, 7A/109031). Phlorizin and empagliflozin were obtained from AdooQ Bioscience. Urea and NH_4HCO_3 were from Acros Organics, Geel, Belgium and trypsin and dimethyl sulfoxide (DMSO) from Thermo Scientific (Waltham, MA). Tris(hydroxymethyl) aminomethane hydrochloride (Tris), LC-MS grade water, acetonitrile and formic acid were obtained from Fisher Scientific (Geel, Belgium).

$CD4^+$ T cells isolation and activation

Peripheral blood mononuclear cells (PBMCs) were isolated by density-gradient centrifugation using Ficoll-Paque™ PLUS (Sigma Aldrich, Sweden). $CD4^+$ T cells were then purified from the isolated PBMCs by negative selection using human$CD4^+$ T cell isolation kits (Miltenyi Biotec, Germany) according to the manufacturer's instructions. The freshly isolated $CD4^+$ T cells (1x 10^6/ml) were suspended in RPMI 1640 glucose-free medium (Gibco, Fisher Scientific, Sweden) supplemented with 2 mM glutamine, 10% heat-inactivated dialyzed fetal bovine serum, 100 U/ml penicillin, 10 mg/ml streptomycin, and 5 μM β-mercaptoethanol (Gibco, Fisher Scientific, Sweden). The activation of the cells was performed in either 96-well (10^5 cell/well) or 24-well (10^6 cell/well) plates based on the purpose of the experiment. $CD4^+$ T cells were activated with 3 μg/ml plate-bound anti-CD3 (BD Biosciences, USA, 555329) in the presence of different concentrations of glucose (2.8 mM, 5.6 mM, 10 mM and 16.7 mM) for 66–72 h and indicated drugs were added based on the experimental design.

MTT Assay

The metabolic activity of $CD4^+$ T cells was assessed in 96-well plates with colorimetric MTT (3-(4,5-Dimethylthiazol-2-yl)-2,5-Diphenyltetrazolium Bromide) assay. It is commonly used to measure cellular metabolic activity based on mitochondrial dehydrogenase in living cells as an indicator of cell viability and proliferation[1]. After 66–72 h of activation, a PBS-soluble tetrazolium dye MTT (final concentration 1mM) was added and incubated for additional 4 h at 37 °C. Thereafter, the cells were centrifuged at 2000 rpm for 10 min to concentrate the insoluble purple formazan pellets. The supernatants were collected and stored at −80 °C for later biomolecules analysis. The formazan crystal pellets were dissolved in DMSO and the plate was read 10 min later using Multiskan FC Microplate Photometer (Thermo Fisher, USA) at 550 nm.

Multiplex Proximity Extension Assay (PEA)

The supernatants collected at the end of the MTT assay were sent on-ice to the SciLifeLab Affinity Proteomics Unit in Uppsala, Sweden, for analysis. Inflammatory proteins were measured using high-throughput multiplex PEA with an Olink Target 96

Inflammatory panel (OlinkProteomics, Uppsala, Sweden). PEA measures simultaneously 92 proteins/biomolecules in different sample matrices where it combines a dual-detection immunoassay and quantitative PCR. Normalized protein expression (NPX) values, an arbitrary unit on the log2 scale, were used to present the data. A protein expression (NPX value) is considered acceptable if the value is above the limit of detection (LOD) for each particular protein. Proteins that were detected in more than 75% of the samples were analyzed in this study: 59 out of 92 proteins had detectable levels. Data for resting, activated and GABA-treated activated $CD4^+$ cells supernatants were analyzed separately. The biomolecules in the supernatants were assessed for each donor at each glucose concentration. The data was computed, processed and analyzed with support from NBIS (National Bioinformatics Infrastructure Sweden). The log2FC (FC =fold change) is the average increase in NPX in GABA as compared to activated alone, this value is both estimated based on the linear mixed effects model and computed as the mean over the GABA-activated difference and plotted in heatmaps. Paired t-test was used followed by multiple testing correction using false discovery rate (FDR) method (Two-stage step-up method of Benjamini, Krieger and Yekutieli) with a threshold 12%.

Determination of IFNγ and IL-10 concentrations in supernatants

The concentrations of IFNγ and IL-10 were measured with enzyme-linked immunosorbent assay (ELISA). The supernatants were diluted when necessary to be in the optimal linear optical range and analyzed using commercial kits for IFNγ (Human IFN-gamma DuoSet ELISA, R&D Systems, USA and Bio legend, UK), and IL-10 (Biolegend, UK) according to manufacturers´ instructions. Optical densities were measured using FC Microplate Photometer (Thermo Fisher, USA) at 450 nm, and 540 nm was used as a correction wavelength. The levels of IFNγ or IL-10 were normalized to controls (activated $CD4^+$ T cells in the absence of drugs).

Total RNA and protein extraction and, bulk RNA sequencing

Total RNA and protein were extracted from activated $CD4^+$ T cells, in the absence or presence of 500 nM GABA, using RNA/Protein Purification Plus Kit (Norgen Biotek, Ontario, Canada). During the extraction process, total RNA was treated with RNase-Free DNase I Kit (Norgen Biotek, Ontario, Canada) to eliminate contamination of genomic DNA. The extracted proteins were quantified using DC protein assay kit (Bio-Rad, USA), and immediately frozen at −80°C. Total RNA samples were submitted to the GENEWIZ NGS facility (Germany) and quality control analysis showed that all RNA samples had an RNA integrity number (RIN) >9 (9.48 ± 0.1, mean ± SEM). Strand-specific RNAseq cDNA libraries with polyA selection were generated and sequenced using Illumina HiSeq sequencing platform (12 samples, 20.8-31.1 million reads, 150 bp paired end per sample). Sequence reads were filtered and trimmed using Trimmomatic V.0.36 to remove low quality reads. The trimmed reads were further mapped and aligned to the Homo Sapiens GRCh38 reference genome (ENSEMBL) using the STAR aligner v.2.5.2b. Unique gene hit counts were calculated using feature Counts from the Subread package v.1.5.2.

Real-Time Quantitative Reverse Transcription (qPCR)

The cDNA was synthesized using SuperScript reverse transcriptase IV (Invitrogen Thermo Scientific, USA) in a 20 µl reaction following the standard protocol from manufacturer. The qPCR reaction was then performed using qPCRBIO SYBR or Probe Mix low-ROX (PCR Biosystems, UK; PB20.11-05), and gene-specific primers

(Table S1) or Taqman probes (*GABRR2* Hs00266703_m1; *IPO8* Hs00914057_m1, ThermoFisher Scientific, USA). Changes in the abundance of each transcript were normalized to the expression of reference genes (*IPO8*). Relative expression levels were calculated by normalizing to non-treated activated $CD4^+$ T cells obtained from the same donor at the same glucose concentration using $2^{-\Delta\Delta Ct}$ method. All samples were run in duplicate. The real-time qPCR amplification was performed in 10 µl reaction mix in a 384-well plate using a QuantStudio™ 5 instrument (ThermoFisher Scientific). All runs started with an initial denaturation step of 2 min at 95 °C, followed by 45 cycles of 95 °C for 5 s and 60 °C for 30 s.

Mass spectrometry (MS)-based bottom-up proteomics

The lysates were purified and tryptic digested for MS-based bottom-up proteomic analysis using Filter Aided Sample Preparation (FASP)[2, 3]. Briefly, 20 µg of total protein were transferred onto centrifugal filter units (Microcon-30 kDa; Merck, Darmstadt, Germany) and washed with a buffer containing 8 M urea and 100 mM Tris (pH 8.5). The washing step was repeated after reduction with 8 mM dithiothreitol (DTT), alkylation with 50 mM iodoacetamide (IAA) and removal excess of IAA with 8 mM DTT. Before tryptic digestion (enzyme-to-protein ratio 1:50 (w/w)) the filter was washed three times with NH_4HCO_3. After incubation in a wet chamber at 37 °C for 16 h the resulting peptides were washed twice from the filter by adding 50 mM NH_4HCO_3. Trifluoroacetic acid was then added to a final concentration of 1% (v/v) and the samples were dried at 45 °C. Finally, the samples were reconstituted in 3% acetonitrile and 0.1% formic acid in water to a final concentration of 150 ng protein/µl. The tryptic peptides were analyzed on a nanoAcquity UPLC system equipped with a C18, 5 µm, 180 µm x 20 mm trap column and an HSS-T3 C18 1.8 µm, 75 µm x 250 mm analytical column (Waters Corporation, Manchester, UK) coupled to a Synapt G2 Si HDMS mass spectrometer with an electrospray ionization source (Waters Corporation, Manchester, UK). The $UDSM^E$ approach with positive ionization was used[2, 3]. Mobile phase A contained 3 % DMSO and 0.1 % formic acid in water and mobile phase B 3 % DMSO and 0.1 % formic acid in acetonitrile. After loading 300 ng of protein on the column in trapping mode, peptide separation was performed with a gradient run from 3 - 40% (v/v) mobile phase B over 120 min. The flow rate was set to 0.3 µl/min and the column oven was set to 40 °C. Method performance was controlled with a commercially available HeLa digest (Thermo Scientific, Waltham, MA). UPLC-MS data processing and label-free quantification: ProteinLynx Global Server (version 3.0.3, Waters Corporation, Milford, MA) was used for raw data processing. With FDR of 10%, a database search against a randomized UniProt human database (Uni-ProtKB version 14/01/2020) was performed. Carbamidomethyl cysteine was set as fixed modification, acetyl lysine, C-terminal amidation, asparagine deamidation, glutamine deamidation and methionine oxidation as variable modifications and trypsin as digest reagent. Minimum peptide matches per protein were 2 and minimum fragment ion matches per peptide and protein were 1 and 3, respectively. For label-free quantification analysis, the identified proteins were further processed using ISOQuant 1.8 as described elsewhere[2]. Following the TOP3 quantification approach the average intensity of the three most intense peptides of each protein were used for relative protein quantification. ISOQuant settings are provided in Table S2.

Immunoblotting

$CD4^+$ T cells were lysed in RIPA buffer (Sigma-Aldrich, R0278) containing protease

inhibitor cocktail (Roche, 11 836 153 001) and phosphatase inhibitors (Sodium orthovanadate, Sigma-Aldrich, S6508). Proteins were heated at 100 °C for 5 min in SDS loading buffer (275 mM Tris. HCL, 9% SDS, 50% glycerol, 0.03% bromophenol blue) containing 9% beta-mercaptoethanol and separated by Mini-Protean TGX gel 4 - 15% (BioRad, stain-free gels #4568084, 4561035) and blotted onto Amersham Hybond-P PVDF membrane. Membranes were blocked with blocking buffer (EveryBlot BioRad, 12010020) for 20 min at room temperature (RT) and incubated overnight at 4 °C with the following primary antibodies: HK1 (GenTex, GTX105248, 1:3000), SGLT2 (ProteinTech, 24654-1-AP, 1:500) and GABRR2 (Invitrogen, PA5-41008, 1:1000). After immunoblotting, membranes were washed in TBST and incubated with Peroxidase-conjugated AffiniPure secondary antibodies (Jackson ImmunoResearch, 111-035-045, 1:5000). Protein detection was done using chemiluminescent ECL reagent (Thermo scientific, 32209). Quantitative densiometric analysis of the immunoblotted bands was performed using Image Labs software (BioRad Laboratories, V6.0.0) and data were normalized for each sample using stain-free technique.

Immunofluorescence staining

$CD4^+$ T cells were harvested after 72 h of anti-CD3 activation on cytoslides (Thermo scientific, 5991056) using a Shandon cytospin centrifuge (400 rpm for 4 min at RT). After drying, cells were fixed with 4% PFA in PBS for 15 min and washed 3 times, followed by membrane permeabilization with 0.1% Triton-X for 5 min. Un-specific binding was blocked with 5% bovine serum albumin and 10% donkey serum (Jackson ImmunoResearch, 017-000121) in 1X PBS for 60 min. Cells were then washed and incubated with primary antibodies diluted in blocking solution overnight at 4 °C followed by incubation with an AlexaFluor 488-conjugated AffiniPure Donkey Anti-Rabbit IgG secondary antibody (Jackson ImmunoResearch, 711-545-152, 1:500) for 1h at RT. Finally, cells were washed again and counterstained with DAPI for 5 min and slides were mounted in ProLongTM Gold antifade reagent (Invitrogen). Images were acquired using confocal microscopy (LSM700, Zeiss) with 63X objective. For statistics, ≥ 50 cells from 3 donors were quantified using ImageJ (NIH) software. Primary antibodies and concentrations included rabbit anti-insulin receptor, InsR (Invitrogen, PA5-29286, 1:800), rabbit anti-GABRR2 (Invitrogen, PA5-41008, 1:600), and rabbit anti-SGLT2 (ProteinTech, 24654-1-AP, 1:100).

***In vitro* Hexokinase activity assay**

Hexokinase activity was measured at RT indirectly as a readout of NADH production, a by-product of the reaction converting glucose-6-phosphate to 6 phosphogluconolacton by the enzyme glucose-6-phosphate dehydrogenase (GPDH). The cells were harvested, centrifugated and washed twice with PBS. Washed cells were resuspended in 1 ml assay buffer solution, on ice, included in the hexokinase enzymatic assay kit (Bio Vision, K789-100). After centrifugation at 4 °C for 5 min, the resulting supernatant was used as the final cell extract for the enzymatic assay.

Electrophysiological recordings

The electrophysiological recordings from the isolated $CD4^+$ T cells were done using the perforated whole-cell patch-clamp configuration. In order to keep the intracellular chloride concentration intact, gramicidin was used to obtain the perforated configuration. Gramicidin was diluted in DMSO at the stock concentration 2 mg/ml and the final concentration of the gramicidin in the pipette solution was 2.6 µg/ml. The

pipette solution with the gramicidin was protected from light, kept cold and used within 2 hours after the preparation. After making the cell-attached configuration, the access resistance was monitored until characteristic slow and low-amplitude capacitance transients were observed and the access resistance decreased from GΩ range to the range of tens of MΩ. The extracellular solution (in mM) contained: 157 NaCl, 4.5 KCl, 0.5 $CaCl_2$, 1 $MgCl_2$, 5 HEPES and 5.6 or 16.7 glucose (pH 7.4, adjusted with NaOH). The pipette solution consisted of (mM): 149 KCl, 2 $CaCl_2$, 1 $MgCl_2$, 1 NaCl, 10 HEPES, 5.6 or 16.7 glucose (pH 7.3 adjusted with KOH). The patch-clamp pipettes were made from borosilicate glass and had a resistance of 12–14 MΩ when filled with the pipette solution and immersed in the extracellular solution. Recordings were done using Axopatch 200B amplifier, filtered at 2 kHz and digitized on-line at 10 kHz using an analog-to-digital converter. To record the electrophysiological data Clampex 10.5 (Molecular Devices, San Jose, CA, USA) software was used. Currents were recorded at +30 mV or by a ramp protocol, where the potential was changed from −80 to +80 mV in 1 s, the holding potential (Vh) was kept −40 mV. The single sweep duration was 20 s with a break between sweeps 5 s. After application of a drug, the chamber was perfused 2-6 min with extracellular solution only before next application of a drug. Currents in the absence of drugs or in the presence of picrotoxin were subtracted from the test-drug current response.

Live cell time-lapse real-time Ca^{2+} imaging

Cells were loaded with a calcium indicator, 3 μM Fluo-8H AM (AAT Bioquest, Pleasanton, CA) for 15 min at 37 °C and seeded on 5% 3-aminopropyltriethoxysilane-coated coverslip for 15 min at 37 °C. Time lapse images were acquired by confocal microscopy (LSM700, Zeiss) with 40X objective at an interval of 1-1.5 second per image. Drugs were diluted in RPMI 1640 without phenol red and perfused at indicated time and concentration by a peristaltic pump. After application of each drug, cells were perfused with the extracellular solution (RPMI 1640) before next application. Area for single cells was marked and absolute fluorescence intensity values (F) were extracted using ZENBlue software. Relative intensity (F/Fmedian) for each cell was calculated for every recorded image and plotted against time. Further, maximum relative intensity of the cells under drug application time is considered as drug's response. Data is represented for all cells and as box-whiskers plot.

Metabolism Assay

Isolated $CD4^+$ T cells were plated in a XF^e96 cell plates that were coated with Cell-Tak (#354240, Corning, New York, USA) according to manufacturer's protocol. The metabolic function of activated $CD4^+$ T cells cultured for 3 days *in vitro* was analyzed by measuring the extracellular acidification rate (ECAR) using an XF^e96 extracellular flux analyzer (Seahorse Bioscience). The cells were kept in XF media (Seahorse Bioscience) supplemented with 5 mM glucose (Sigma Aldrich), and subjected to glycolysis stress-test protocol using sequential injection of 25 mM glucose, 2 μM oligomycin, and finally 15 mM 2-deoxyglucose (2DG). Measurements for each experiment were conducted at least in triplicates and glycolysis, glycolytic capacity, and glycolytic reserve calculated and values normalized to protein content [4, 5].

Glucose uptake assay

2x 10^6 activated $CD4^+$ T cells (72 h activation) with insulin treatment from 48 h after activation were pelleted, resuspended in glucose-free RPMI-1640 media, incubated for 10 min in the incubator at 37 °C, and washed once with the same media. Glucose-

free media (500 μl) containing 1μCi/ml [^{14}C] glucose (Perkin Elmer) were added to cells in the absence or presence of phlorizin (100 μM) or empagliflozin (0.5 μM). Cells were incubated for 40 min at 37 °C, pelleted by centrifugation at 300x g for 5 min and washed three times in cold PBS. Cells were then lysed in RIPA buffer and ^{14}C content was measured with Gold XR scintillation fluid using a liquid scintillation counter (Perkin Elmer). The glucose uptake was calculated by normalizing counts to protein contents for each sample.

Statistical analysis

Statistical analysis was performed using GraphPad Prism 9 GraphPad Prism (GraphPad Software Inc., La Jolla, CA, Version 9.3.1). Normalized PEA data were assessed by two-tailed paired t-test followed by Benjamini-Hochberg's FDR (False Discovery Rate) method. The significance level is set to 10% FDR. Cellular metabolic activity, cytokine levels, mRNA, protein expression and ECAR of CD4^{+} T cells in the presence of indicated drugs were normalized to controls (activated cells without drug treatment) from each donor and for each glucose concentration. Normalized data were analyzed by one-sample t-test when compared to controls. A comparison between paired groups was performed using repeated measures or mixed-model effects one-way ANOVA followed by Tukey or Fisher's LSD multiple comparisons tests. Unpaired multiple-group comparison was performed using ordinary one-way ANOVA followed by Tukey test. Changes in protein levels in MS data were analyzed using Quantitative, multi-dataset Pathway Analysis (ReactomeGSA, https://reactome.org/PathwayBrowser/#TOOL=AT)[6] and volcano plot was subsequently generated. Error bars in the bar graphs represent SEM unless otherwise specified and the statistical significance level was set to 0.05.

Additional references

1. Morgan DM. Tetrazolium (MTT) assay for cellular viability and activity. *Methods Mol Biol*, **79**, 179-183 (1998).
2. Rofo, F. *et al.* Wide-Ranging Effects on the Brain Proteome in a Transgenic Mouse Model of Alzheimer's Disease Following Treatment with a Brain-Targeting Somatostatin Peptide. *ACS Chem Neurosci* **12**, 2529-2541 (2021).
3. Distler, U., Kuharev, J., Navarro, P. & Tenzer, S. Label-free quantification in ion mobility-enhanced data-independent acquisition proteomics. *Nat Protoc* **11**, 795-812 (2016).
4. Pelletier, M., Billingham, L.K., Ramaswamy, M. & Siegel, R.M. Extracellular flux analysis to monitor glycolytic rates and mitochondrial oxygen consumption. *Methods Enzymol* **542**, 125-149 (2014).
5. Traba, J., Miozzo, P., Akkaya, B., Pierce, S.K. & Akkaya, M. An Optimized Protocol to Analyze Glycolysis and Mitochondrial Respiration in Lymphocytes. *J Vis Exp* (2016).
6. ReactomeGSA - Efficient Multi-Omics Comparative Pathway AnalysisJohannes Griss, Guilherme Viteri, Konstantinos Sidiropoulos, Vy Nguyen, Antonio Fabregat, Henning Hermjakob. bioRxiv 2020.04.16.044958; doi: https://doi.org/10.1101/2020.04.16.044958